Deanship of Graduate Studies
Al-Quds University

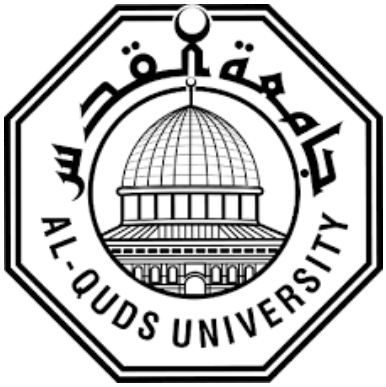

Centrifugal Acceleration at High Altitudes above the Polar Cap: A Monte-Carlo Study

Hamza Ahmad Mohammad Abudayyeh

M.Sc. Thesis

Jerusalem, Palestine

1436-2015

Centrifugal Acceleration at High Altitudes above the Polar Cap: A Monte-Carlo Study

Prepared By:
Hamza Ahmad Mohammad Abudayyeh

B.Sc.: Birzeit University, Palestine

Supervisor: Prof. Imad A. Barghouthi.

This thesis is submitted in partial fulfilment of the requirements for the degree of Master of Science from the Department of Physics, Faculty of Science and Technology, Al-Quds University.

1436-2015

Al-Quds University
Deanship of Graduate Studies
Department of Physics

Thesis Approval

Centrifugal Acceleration at High Altitudes above the Polar Cap: A Monte-Carlo Study

Prepared By: Hamza Ahmad Mohammad Abudayyeh
Registration No: 21311887

Supervisor: Prof. Imad A. Barghouthi.

Master thesis submitted and accepted, Date: **25 July 2015**
The names and signatures of the examining committee members are as follows:

1- Head of Committee:	Prof. Imad A. Barghouthi	Signiture: _____
2- Internal Examiner:	Dr. Husain R. Alsamamra	Signiture: _____
3- External Examiner:	Dr. Lilia A. Mashal	Signiture: _____

Jerusalem, Palestine

1436 AH/2015 AD

.

Dedication

I dedicate this thesis to my father, mother, wife and child, for their encouragement and trust

Declaration

I certify that this thesis submitted for the degree of Master, is the result of my own research, except where otherwise acknowledged, and that this study (or any part of the same) has not been submitted for a higher degree to any other university or institution.

Signed:

Hamza Ahmad Mohammad Abudayyeh

Date: 25 July 2015

Acknowledgments

Praise be to Allah the Beneficent, the Merciful, for enabling me to complete this study and may peace and blessings be upon the prophet Mohammad. I would like to present my deepest appreciation to whoever assisted me in any form to complete this study. I would especially like to thank my research supervisor Prof. Imad Barghouthi for his unlimited support and for teaching me all the vital skills throughout the course of my study. I would also like to thank the Swedish Institute for Space Physics and Lulea University of technology; especially Prof. Hans Nilsson and Dr. Rikard Slapak for their assistance and for their generous grant to visit their institutes. I would like to express my deepest gratitude to my father and mother, who are my greatest supporters throughout my life. I would also like to extend my appreciation to my wife and my son Ahmad who have supported me and endured my absence during my studies.

Abstract

A Monte Carlo simulation was used to study the outflow of O^+ and H^+ ions along three flight trajectories above the polar cap up to altitudes of about 15 R_E. *Barghouthi* (2008) developed a model on the basis of altitude and velocity dependent wave-particle interactions, and a radial geomagnetic field which includes the effects of ambipolar electric field and gravitational and mirror forces. In the present work we improve this model to include the effect of the centrifugal force, with the use of relevant boundary conditions. In addition,the magnetic field and flight trajectories, namely the central polar cap (CPC), nightside polar cap (NPC) and cusp, were calculated using the Tsyganenko T96 model. To simulate wave-particle interactions, the perpendicular velocity diffusion coefficients for O^+ ions in each region were determined such that the simulation results fit the observations. For H^+ ions, a constant perpendicular velocity diffusion coefficient was assumed for all altitudes in all regions as recommended by *Nilsson et al.* (2013). The effect of centrifugal acceleration was simulated by considering three values for the ionospheric electric field: 0 (no centrifugal acceleration), 50, and 100 mV/m. It was found that the centrifugal acceleration increases the parallel bulk velocity and decreases the parallel and perpendicular temperatures of both ion species at altitudes above about 4 R_E. Centrifugal acceleration also increases the temperature anisotropy at high altitudes. At a given altitude, centrifugal acceleration decreases the density of H^+ ions while it increases the density of O^+ ions. This implies that with higher centrifugal acceleration more O^+ ions overcome the potential barrier. It was also found that aside from two exceptions centrifugal acceleration has the same effect on the velocities of both ions. This implies that centrifugal acceleration is universal for all particles. The parallel bulk velocities at a given value of ionospheric electric field were highest in the cusp followed by the CPC followed by the NPC. In this study a region of no wave-particle interaction was assumed in the CPC and NPC between 3.7 and 7.5 R_E. In this region the perpendicular temperature was found to decrease with altitude due to perpendicular adiabatic cooling.

Contents

List of Tables

List of Figures

Chapter 1

General Introduction

In this chapter a very concise introduction will be presented. For more information and for proofs and rigorous details refer to *Baumjohann and Treumann* (1996); *Chen and Trivelpiece* (1976); *Walt* (2005), from which most of the material in this chapter is derived from.

1.1 Basic Plasma Physics

A plasma is an ionized gas which contains roughly the same number of positive and negative charge carriers. Although on earth, plasmas are quite rare, more than 99% of all baryonic matter in the universe is in the plasma state. Since positive and negative charges attract, a plasma typically cannot maintain in its ionized state unless it has temperatures (usually denoted by T) of a few electronvolts (eV). [1] [2]

Equal numbers of positive and negative charge carriers in a volume element are necessary for the plasma to behave *quasineutral* in the stationary state. This means that on average the electric fields resulting from every charge seem to cancel on large enough scales. To understand this effect, we may consider for example one charge. Typically in free space this

[1] In plasma physics it is typical to use units of eV for temperature even though it is a unit of energy. In this system of units the Boltzmann constant (k_B) is set to 1, or in other words when we say temperature we actually mean thermal energy ($k_B T$) and this notation will be used for the remainder of the thesis

[2] 1 eV = 11605 Kelvin (K)

charge would generate a coulomb potential. However, since there are 'free' charges in the neighborhood, this coulomb potential is shielded and transforms into the *Debye potential* form

$$\phi_D = \frac{q}{4\pi\epsilon_0 r} e^{-\frac{r}{\lambda_D}}$$

with ϵ_0 being free space permittivity, q being the charge of the charge carrier, and r being the distance from the charge carrier. The exponential function causes the potential to die away at distances $r > \lambda_D$. The length λ_D is called the *Debye length*, and is a characteristic length scale of the plasma. The Debye length is the distance needed for proper shielding to occur. This means that if we look at length scales much larger than the Debye length, the plasma appears to be neutral; whereas if we look at length scales smaller than λ_D then the plasma will appear to have local electrical charge distributions. Therefore, to deal with plasmas the physical dimension of the system $L >> \lambda_D$. The Debye length depends on the electron and ion temperatures, T_e and T_i, and the plasma density, $n_e \simeq n_i$ (assuming singly charged ions) (see *Chen and Trivelpiece*, 1976; *Baumjohann and Treumann*, 1996):

$$\lambda_D = \sqrt{\frac{\epsilon_0 T_e}{n_e e^2}}$$

where we assumed that $T_e \simeq T_i$ and where e is the electron charge.

For collective shielding to occur, the number of ions in a sphere of radius λ_D (called the Debye sphere) must be large. The number of particles in a Debye sphere is $\frac{4\pi}{3} n_e \lambda_D^3$. Therefore, we may define the *plasma parameter* $\Lambda = n_e \lambda_D^3$ and it must be much larger than 1.

If the quasineutrality of the plasma is perturbed by some external force then the electrons (being much lighter than the ions) will be accelerated towards the equilibrium position, this will result in an oscillatory motion about the equilibrium position with a characteristic frequency ω_{pe} called the *plasma frequency* given by (see *Chen and Trivelpiece*, 1976;

Baumjohann and Treumann, 1996):

$$\omega_{pe} = \sqrt{\frac{n_e e^2}{m_e \epsilon_0}}$$

where m_e is the electron mass. Some ionized media are not fully ionized like the ionosphere. In such a case during this oscillation, electrons may collide with neutrals and may be forced into an equilibrium with neutrals and the medium will no longer behave as a plasma. Therefore to maintain a plasma the average time between two electron-neutral collisions , τ_n, must be much larger than the oscillation period $\left(\frac{1}{\omega_{pe}}\right)$. To summarize, for an ionized medium to behave like a plasma, three criteria must be satisfied:

1. $\lambda_D \ll L$
2. $\Lambda \gg 1$
3. $\omega_{pe}\tau_n \gg 1$

The study of plasma dynamics is complex since not only external fields govern the motion of the plasma; the motion of ions inside the plasma also generate fields which themselves affect the total dynamics of the system. In principle, one can study the motion of every single particle in the plasma which yields a large number of coupled equations of motion that must be solved simultaneously. This approach is not only extremely complex, but the outputs would be of no use since the quantities of interest are usually macroscopic quantities like the density and temperature. Therefore, for each case a certain approximation is used and several approaches are followed to study the dynamics of plasmas.

The most basic and simple approach is the *single particle motion* description. The motion of a single particle is considered under the effect of external fields only. The total motion of the plasma is assumed to be similar to the motion of the single particle. This approach neglects the interactions between plasma particles and therefore internal fields. Hence this method is very useful only in very low density plasmas as in some geophysical plasmas.

The *magnetohydrodynamic* (MHD) approach treats the plasma as a single conducting fluid with macroscopic variables like average density, velocity, and temperature. This approach neglects all single particle aspects and assumes that local equilibrium is achieved and therefore is only suitable for low-frequency influences. A small improvement on this approach is to treat every particle species (electrons, protons, ...etc) as a separate fluid. This is called the *multi-fluid* approach and it enables the distinction between the motion of lighter electrons and heavier ions.

The *kinetic theory* is the most developed approach. Instead of looking at the motion of each particle, it looks at the development of the distribution function of the system in phase space. Therefore this approach is a statistical approach which makes it the most accurate method for plasmas.

1.1.1 Single Particle Motion Description

This approach is relatively simple since the only equation that has to be solved is Newton's second law, incorporating the appropriate external forces. Typically the most important force in consideration is the Lorentz force. In some such situations (such as motion of heavy ions in geophysical plasmas) gravitational forces may be significant. However since the effect of gravity is trivial, it will not be considered in this subsection.

If an external magnetic field is present near or in a plasma, it introduces a preferred direction. Therefore, all vector quantities in this study will be divided into two components: a component parallel to the external magnetic field (one degree of freedom); and a component perpendicular to the magnetic field (2 degrees of freedom). For example, the velocity of a particle, $\mathbf{v}$, may be decomposed to a parallel component ($v_{\|}$) and a perpendicular component ($v_{\perp}$).

If a charge q of mass m with velocity $\mathbf{v}$ enters a region of uniform magnetic field, $\mathbf{B}$, with an angle of α between the velocity and magnetic field, then it is well known that the ion will experience a central force perpendicular to the local magnetic field. This force will

cause the perpendicular component of the velocity to constantly change its direction in the perpendicular plane and therefore form a circular motion whose center is called the *guiding center*. The parallel component of the velocity however, will not experience any acceleration; therefore the total motion of the particle would be a helix of pitch angle α about a magnetic field line. The radius of gyration, r_g, gyrofrequency, Ω_g, and pitch angle are given by:

$$r_g = \frac{mv_\perp}{qB} \tag{1.1}$$

$$\Omega_g = \frac{qB}{m} \tag{1.2}$$

$$\alpha = \arctan \frac{v_\perp}{v_\parallel} \tag{1.3}$$

If an electric field is also present in the region then we can also decompose it to parallel and perpendicular components, $E_\parallel$ and $E_\perp$. The parallel component of the electric field will only result in a field-aligned acceleration, while the perpendicular component will cause the guiding center to drift with a uniform velocity, $\mathbf{v}_E$ given by:

$$\mathbf{v}_E = \frac{\mathbf{E} \times \mathbf{B}}{B^2} \tag{1.4}$$

which is usually called the E×B drift. The E×B drift is independent of the sign of the charge and thus electrons and positive ions drift in the same direction.

This expression for the drift may be generalized to any perpendicular force field , $\mathbf{F}$, by:

$$\mathbf{v}_F = \frac{1}{q}\frac{\mathbf{F} \times \mathbf{B}}{B^2} \tag{1.5}$$

An important example of a general force is the gradient force:

$$\mathbf{F}_\nabla = -\mu \boldsymbol{\nabla} B \tag{1.6}$$

When the gradient of the magnetic field is along the magnetic field direction (i.e. the magnetic

field is increasing or decreasing), the force always points towards weaker field regions, and is called the *mirror force*.

As the ion gyrates about the guiding center it has a magnetic dipole moment, μ, given by:

$$\mu = \frac{mv_\perp^2}{2B} = \frac{W_\perp}{B} \tag{1.7}$$

where $W_\perp = \frac{1}{2}mv_\perp^2$ is the perpendicular energy of the particle. When the time variations of the external fields are much smaller than the *gyroperiod* ($\frac{1}{\Omega_g}$), then the magnetic moment will not change substantially from one period to another and may be assumed to be constant. The magnetic moment in this case is called the *first adiabatic invariant*. The conservation of the first adiabatic invariant is essential in understanding the bounce motion of ions in the magnetosphere. Suppose that an ion is moving along a geomagnetic line towards earth. While moving closer, it experiences higher magnetic fields; but in order to conserve the magnetic moment the perpendicular velocity must also increase. However, in the absence of electric fields the total energy must be constant since magnetic fields do no work. Therefore the increase of perpendicular velocity leads to a decrease in the parallel velocity. If the field keeps increasing, the ion will reach to a point where it possesses no parallel velocity, however the mirror force points in the opposite direction and therefore the particle bounces back. The point at which this bounce occurs is called the mirror point. The ion may however be lost if the mirror point is so low that the ion enters a collision dominated region, where the ion collides with atmospheric particles. The exact opposite happens while traveling to weaker field regions, as the perpendicular velocity is transformed into parallel velocity in a phenomenon called perpendicular adiabatic cooling.

1.1.2 Kinetic Theory

In kinetic theory, a statistical approach is adopted and hence the development of the plasma is described in terms of the distribution function for the system of particles in phase space. The distribution function, $f(\mathbf{r}, \mathbf{v}, t)$, is defined as the number of particles at time t which

have velocities between $\mathbf{v}$ and $\mathbf{v} + \mathbf{dv}$ and are located at distances between $\mathbf{r}$ and $\mathbf{r} + \mathbf{dr}$. From this distribution function the macroscopic quantities of the plasma may be found (see *Barakat and Lemaire*, 1990). These quantities include the average density, bulk velocity, and perpendicular and parallel temperatures. The parallel and perpendicular temperatures contain information about the average kinetic energy in the parallel and perpendicular directions.

It is convenient to assign each ion species a distribution function $f_s(\mathbf{r}, \mathbf{v}, t)$, where the subscript s indicates the ion species. Considering a general force, $\mathbf{F}$, acting on the plasma; the development of the distribution function is described by the well-known Boltzmann equation (*Schunk*, 1977):

$$\frac{\partial f_s}{\partial t} + \mathbf{v_s}.\boldsymbol{\nabla} f_s + \frac{1}{m_s}\mathbf{F}.\boldsymbol{\nabla}_{v_s} f_s = \frac{\delta f_s}{\delta t} \tag{1.8}$$

where $\mathbf{v_s}$ and m_s are the velocity and mass of the s^{th} species respectively; $\boldsymbol{\nabla}$ and $\boldsymbol{\nabla}_{v_s}$ are the gradient in space and velocity coordinates respectively; and $\frac{\delta f_s}{\delta t}$ represents the rate of change of the distribution function in a given region of phase space as a result of collisions and wave-particle interactions.

1.2 The Space Environment

The earth is the third planet from the sun, the densest planet of our solar system, and the largest of the four solar system's terrestrial planets. Earth rotates around the sun in an elliptical orbit with a mean distance of 1 AU=1.5×10^8 km and with a speed of nearly 30 km/s relative to the sun. It is well known that the sun is the source of nearly all light in the solar system. However, what is less known is that the sun also ejects enormous amounts of high speed ions into the solar system in what is known as the solar wind.

The expansion of the solar corona results in the ejection of a highly conductive plasma with supersonic speeds ($\sim$ 500 km/s) into interplanetary space. Since the solar wind originates

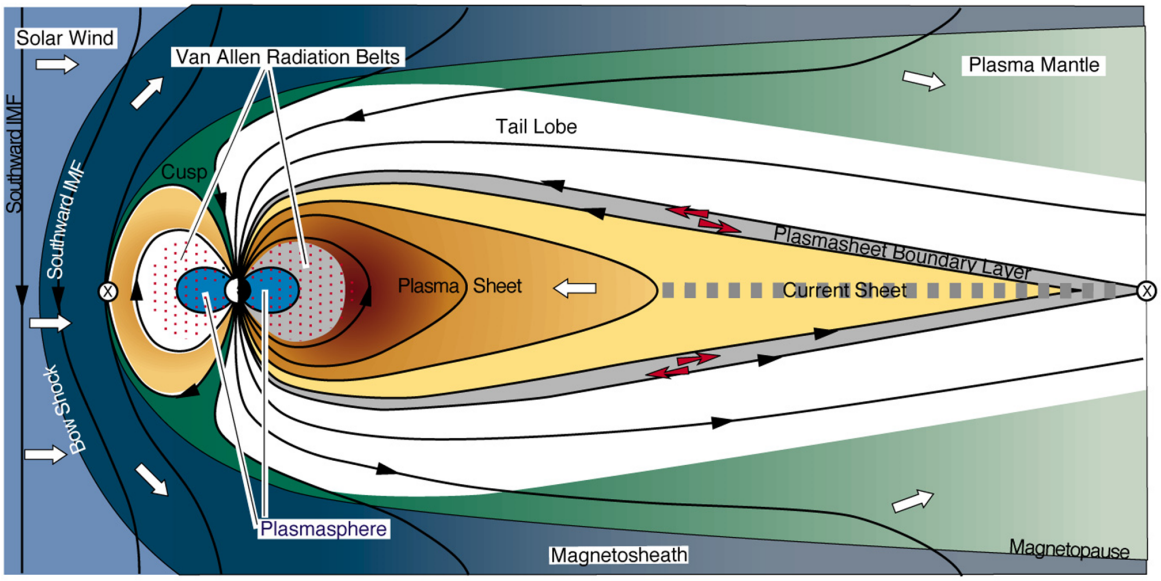

Figure 1.1: Schematic view of the magnetosphere

from the outer layers of the sun, its main components are electrons and protons with a typical density and temperature of about 5 cm^{-3} and 10 eV respectively. Due to its high conductivity, solar magnetic field lines get frozen into the plasma while it is ejected. Consequently, as the solar wind drives into interplanetary space, it drags with it solar magnetic field lines forming what is called the *interplanetary magnetic field* (IMF) which is of the order of 5 nT.

Earth's magnetosphere is a region of space containing terrestrial magnetic field lines which originate from electric currents in Earth's core. Without external influences the terrestrial magnetic field is a dipole field with moment pointing to the north magnetic pole. The impinging solar wind plasma however, causes the magnetic field lines to be compressed in the sunward direction and then flows around the magnetic barrier and elongates field lines in a tail that extends several million kilometers in the antisunward direction as shown in figure 1.1. Since the solar wind speed is supersonic before it hits Earth's magnetosphere, a shock wave, called the *bow shock*, is formed 2-3 earth radii (R_E)[3] from the magnetic barrier. The barrier that separates the plasma that is of solar origin from that which is of terrestrial origin is called the *magnetopause*. The region between the magnetopause and the bow shock is called the *magnetosheath* in which the solar wind ions are reduced to subsonic speeds.

[3] 1 R_E = 6371 km is the mean radius of the solid earth

Due to this sudden change of speed, most of the kinetic energy of the solar wind plasma is converted to thermal energy.

Figure 1.1 is a simplified schematic of Earth's magnetosphere. The purpose of this illustration is to point out the different regions of the magnetosphere and their approximate locations. In this thesis we are especially concerned with the outflow of ions along magnetic field lines originating from the polar cap. The polar cap is defined as the region from which the magnetic field lines extend into the tail region of the magnetosphere (sometimes called open field lines). As seen in figure 1.1, the polar cap is a high latitude region around the magnetic poles. The cusp is the high latitude region at which the magnetic field lines diverge, which causes an open route where the solar wind plasma can enter the magnetosphere. For a more detailed morphology of the magnetosphere refer to *Baumjohann and Treumann* (1996).

1.3 Acceleration Mechanisms

In this thesis we will be focusing on the outflow of ions from the topside of the ionosphere (hereinafter referred to as the exobase). Ions of ionospheric origin are not merely adiabatically transported along field lines under the effect of the mirror force alone. On the contrary, heavier ions that initially have velocities well below the escape velocity are observed at high altitudes. Moreover the perpendicular temperatures of H^+ and O^+ ions are observed to increase with altitude in some regions of the polar cap, which contradicts with the conservation of the first adiabatic invariant. This leads to the conclusion that outflowing ions are accelerated along their path. Several acceleration mechanisms were proposed which are divided into parallel acceleration mechanisms such as field-aligned electric fields, gravity (deceleration mechanism), and centrifugal acceleration; and perpendicular acceleration mechanisms such as wave-particle interaction. In this section a brief description of these mechanisms is presented.

The most important of field-aligned electric fields is the *ambipolar electric field*. The ambipolar electric field is a result of the higher mobility of electrons in a plasma. As the

plasma is accelerated, electrons gain more velocity than ions due to their small mass; therefore negative and positive ions are separated and an electric potential forms. By solving Poisson's equation, the potential, ϕ_{am}, takes the form (see *Chen and Trivelpiece*, 1976):

$$\phi_{am} = T_e \ln\left(\frac{n_e}{n_{e0}}\right)$$

where T_e is the electron temperature[4], n_e is the electron density at altitude r , n_{e0} is the electron density at the injection point. The quasineutrality condition implies that the electron density must be equal to the sum of the densities of positive ions.

The effect of body forces (i.e. the ambipolar electric force and gravitational force) is given by the potential Φ (*Barghouthi*, 1997):

$$\Phi = T_e \ln\left(\frac{n_e}{n_{e0}}\right) + GM_E m_s \left(\frac{1}{r_0} - \frac{1}{r}\right) \tag{1.9}$$

where G is Newton's gravitational constant , M_E is the mass of the earth and r_0 is the altitude of the injection point. Here we have set the zero of potential at the injection point.

In addition to the body forces the plasma experiences effects such as the mirror force, centrifugal acceleration and wave-particle interaction. The mirror force is a result of a diverging magnetic field and the conservation of the first adiabatic invariant. The latter two effects will be discussed in more detail in the following two subsections.

1.3.1 Centrifugal Acceleration

The mechanism of centrifugal acceleration was first discussed by *Cladis* (1986) . This acceleration arises from the change of direction of the magnetic field in the presence of a finite convection electric field. This can clearly be seen by decomposing the velocity of the ion to a drift velocity ($\mathbf{V_d}$) and a velocity parallel to the magnetic field ($v_{||}$):

[4]Remember temperatures are given in units of energy in this thesis and therefore k_B is explicitly set to 1.

$$\frac{d\mathbf{R}}{dt} = \mathbf{V_d} + v_{||}\hat{\mathbf{b}} \tag{1.10}$$

where $\mathbf{R}$ is the position vector of the guiding center of the ion and $\hat{\mathbf{b}}$ is a unit vector in the direction of the magnetic field. Since the most dominant component of the drift velocity is the E×B drift we will neglect the other components and consider only the E×B drift velocity $\mathbf{V_E} = (\mathbf{E} \times \mathbf{B})/B^2$. For a simple convection resulting from a dawn-dusk convection electric field, the ion experiences centrifugal acceleration due to the change of the magnetic field direction while the ion moves transverse to the magnetic field. The parallel acceleration may be given by:

$$\frac{d}{dt}(\hat{\mathbf{b}}.\frac{d\mathbf{R}}{dt}) = \frac{dv_{||}}{dt} + \mathbf{V_E}.\frac{d\hat{\mathbf{b}}}{dt} \tag{1.11}$$

The first term on the right hand side of equation 1.11 is the acceleration due to other field aligned magnetic fields such as the polarization electric field, mirror force, and the gravitational field. The second term is the centrifugal acceleration term a_c and by expanding the full derivative we obtain the expression given by *Cladis* (1986) :

$$a_c = \mathbf{V_E}.\left(\frac{\partial\hat{\mathbf{b}}}{\partial t} + v_{||}\frac{\partial\hat{\mathbf{b}}}{\partial s} + (\mathbf{V_E}.\nabla)\hat{\mathbf{b}}\right) \tag{1.12}$$

where $\mathbf{s}$ is a vector along the magnetic field. We will refer to the first term on the right hand side of equation 1.12 (the $\mathbf{V_E}.\frac{\partial\hat{\mathbf{b}}}{\partial t}$ term) as the temporal term. The second term ($v_{||}\mathbf{V_E}.\frac{\partial\hat{\mathbf{b}}}{\partial s}$) will be denoted the parallel term and the third term ($\mathbf{V_E}.(\mathbf{V_E}.\nabla)\hat{\mathbf{b}}$) will be called the perpendicular term. The temporal term depends on the E×B drift and the temporal change of the magnetic field while the perpendicular term depends the E×B drift and the spatial derivative of the magnetic field, and both terms are universal for all particles. The parallel term depends on the particular ion species through the parallel velocity $v_{||}$. To be useful for models the parallel term must be decomposed into the parallel velocity and a species-independent factor $\mathbf{V_E}.\frac{\partial\hat{\mathbf{b}}}{\partial s}$

which will be henceforth called the partial parallel term and has units of inverse time. Since

$$\frac{\partial \hat{\mathbf{b}}}{\partial s} = -\boldsymbol{\kappa} \tag{1.13}$$

where $\boldsymbol{\kappa} = \mathbf{R_c}/R_c^2$ (R_c is the radius of curvature) is the curvature vector of the magnetic field line, it is evident that the parallel term is positive when the curvature is anti-parallel to $\mathbf{V_E}$. This is generally the case along the meridional plane above the polar cap.

The total centrifugal acceleration experienced by a particle will not generally be dependent on its velocity along its path and hence the initial velocity at the injection point. *Nilsson et al.* (2010) discussed the effect of initial velocity on the total centrifugal acceleration. They found that since the time spent being accelerated is inversely proportional to the velocity and the parallel term of the centrifugal acceleration is linearly dependent on the velocity, the two effects offset. Slower particles will spend more time being accelerated by the perpendicular term while faster particles will be accelerated more by the parallel term but will have less time to be accelerated.

Nilsson et al. (2008) reported that the temporal term has a distribution that is almost uniformly distributed in the negative and positive regions and on average is nearly zero. They also reported that the perpendicular term is usually larger than the parallel term but they are equally important.

1.3.2 Wave-Particle Interactions (WPI)

The presence of high perpendicular temperatures and high velocities at high altitudes is an indication of local transverse heating at those altitudes (*Nilsson et al.*, 2012, 2013). This may be explained using resonant wave-particle interactions. Broad-band low frequency waves with frequencies ranging from less than 1 Hz to several hundred Hz and whose electric field component is perpendicular to the magnetic field may be able to heat the ions in the transverse direction (*André and Yau*, 1997; *Waara et al.*, 2011). For such heating to occur the frequency

of the wave must be equal to the ion gyrofrequency or one of its harmonics. Since the ion is moving along the magnetic field line the Doppler shift must be taken into account and in reality the particle detects the wave at the Doppler shifted frequency. Thus the condition for this resonance can be written as (*Tsurutani and Lakhina*, 1997):

$$\omega - \mathbf{k}.\mathbf{v} = n\Omega$$

where ω and $\mathbf{k}$ are the wave frequency and the wave vector, n is an integer and Ω is the gyrofrequency of the ion. If we consider waves moving along the magnetic field lines and considering the fundamental resonance mode, this condition reduces to:

$$\omega - k_{||}v_{||} = \Omega$$

For positive ions only left-hand polarized waves can heat the ions. The ion cyclotron heating rate may be computed using a model given by *Chang et al.* (1986):

$$\frac{dW}{dt} = \frac{q^2}{2m}S_L$$

where q_s and m_s are the charge and mass of the s^{th} species, and S_L is the electric field spectral density at the ion gyrofrequency that is efficient in heating the ions.

For use in kinetic models the heating rate needs to be written in terms of a quasi-linear velocity diffusion coefficient. One way to achieve this is to represent the effect of wave particle interaction as a diffusion in velocity space. In the absense of collisions the right-hand side of equation 1.8 may be given by (*Barghouthi et al.*, 1994):

$$\frac{\delta f_s}{\delta t} = \frac{1}{v_\perp}\frac{\partial}{\partial v_\perp}\left(D_{\perp s}v_\perp\frac{\partial f_s}{\partial v_\perp}\right) \tag{1.14}$$

where $v_\perp$ is the velocity of the ion perpendicular to the magnetic field and $D_{\perp s}$ is the quasi-linear velocity diffusion rate perpendicular to the magnetic field for the s^{th} species.

The perpendicular velocity diffusion coefficient ($D_{\perp s}$) can be written as (*Retterer et al.*, 1987):

$$D_{\perp s} = \frac{q_s^2}{4m_s^2}|S_L| \tag{1.15}$$

The fraction of spectral density at the ion gyrofrequency that is efficient in heating the ions is often denoted as η and therefore $S_L = \eta S$, where S is the total spectral density at the ion gyrofrequency. If the spectral density was measured in the rest frame of the ions, η would correspond to the fraction of left-hand polarized waves which is usually close to 50%. Since the spectral density is measured in the reference frame of the spacecraft this fraction is usually less than 50%. At lower altitudes values for η ranging from a few percent to 10 % were used in several studies (*Barghouthi and Atout*, 2006; *Bouhram et al.*, 2004). *Nilsson et al.* (2013) found that at altitudes between 8 R_E and 10 R_E in the central polar cap and cusp, good agreement was attained for a value of η equal to $\frac{1}{2}$.

For reviews on the theory and observations of WPI see *André and Yau* (1997); *Andre* (1997); *Tsurutani and Lakhina* (1997); and *Moore and Horwitz* (2007).

Chapter 2

Literature Review

The escape of gravitationally bound ions from the polar region of the ionosphere plays an important role in the dynamics of the magnetosphere. The existence of heavy ions at high altitudes that were initially well below the escape velocity at ionospheric altitudes suggests further energization along the particle trajectories. The presence of O^+ ions at magnetospheric altitudes was first discovered by *Shelley et al.* (1972). Since then the presence of O^+ ions at distances of several earth radii with bulks velocities of some tens of km/s was confirmed by using the DE-1 satellite (*Lockwood et al.*, 1985; *Horwitz and Lockwood*, 1985), the Cluster spacecraft (*Nilsson et al.*, 2004), and the Interball-2 Satellite (*Chugunin*, 2009). Several acceleration mechanisms, such as wave-particle interaction (WPI) (*Chang et al.*, 1986) and centrifugal acceleration (*Cladis*, 1986), were introduced in order to explain this phenomenon. Whether outflowing plasma escapes or not depends on how effectively the plasma is accelerated along its trajectory. Low energy ions will convect towards the plasma sheet, but if the ions are sufficiently energized they will pass the tail reconnection point and escape into the solar wind. O^+ ions in the lobes are observed as cold beams (*Seki et al.*, 1998; *Liao et al.*, 2010). The highest fluxes of O^+ in the magnetosphere are however observed in the high altitude cusp and mantle (*Nilsson*, 2011), with enhanced perpendicular temperatures and with parallel velocities sufficiently high to eventually escape. Recent studies by *Slapak et al.* (2012, 2013) also show that a significant amount of O^+ escapes into the dayside magnetosheath

directly from the cusp after being greatly energized along its trajectory in the cusp. Modeling ion outflow and reproducing observations is therefore an important part in order to understand the global dynamics of the magnetosphere. Incorporating different acceleration mechanisms, many models were suggested to study the plasma outflow (*Bouhram et al.*, 2004; *Demars and Schunk*, 1992, 1994; *Demars et al.*, 1996, 1999; *Demars and Schunk*, 2002; *Horwitz et al.*, 1994; *Barakat and Barghouthi*, 1994; *Barakat et al.*, 1998; *Barakat and Schunk*, 2006; *Barghouthi*, 1997; *Barghouthi et al.*, 2003, 2007, 2011, 2012, 2014). For a review on the history of the polar wind models and observations see *Lemaire et al.* (2007) and for a recent review of the kinetic modeling of the polar wind see *Tam et al.* (2007).

By tracking individual particle trajectories, the effect of a convection electric field in accelerating ions in the polar region was first studied by *Cladis* (1986). Only the motion along the noon-midnight meridional plane was considered to simplify the convection electric field. *Cladis* (1986) found that centrifugal acceleration can increase the outflow velocities of ions by more than one order of magnitude. Collective effects such as polarization electric fields could not be studied by *Cladis* (1986) and therefore his study is not directly applicable to the polar wind. Nevertheless his study was an indication of the importance of centrifugal acceleration in the dynamics of the polar wind.

Horwitz et al. (1994) used a time-dependent semi-kinetic model of the polar plasma outflow which included the effects of the ambipolar electric field, mirror force, gravitational force, and centrifugal acceleration. They considered ionospheric electric fields of 10, 50, and 100 mV/m and different exobase temperatures. The magnetic field was modeled by a dipole field and the motion was considered along the meridional line at a latitude of 90°. They also considered longitudinal convection along constant L-shells. In both cases it was found that the effect of the magnetic field curvature on centrifugal acceleration can be neglected. *Horwitz et al.* (1994) found that O^+ bulk velocity increased from 0 km/s at 4000 km altitude to about 10 km/s at 5 R_E for a 50 mV/m ionospheric convection electric field. The change of O^+ density was found to be dependent on the exobase temperature. At low exobase temperatures the density significantly increased with higher ionospheric electric fields, while for high exobase

temperatures the density decreased slightly with increasing ionospheric electric fields.

Demars et al. (1996) used a macroscopic particle in cell (PIC) model coupled with a time-dependent three dimensional hydrodynamic model of the polar ionosphere to investigate the effect of centrifugal acceleration on the plasma outflow at high latitudes. Their study included the effects of electrostatic electric fields, gravitational, mirror and centrifugal forces and for different exobase ion and electron temperatures. The effect of centrifugal acceleration was studied for both steady state and time dependent simulations.It was found that the effect of centrifugal acceleration was negligible on the outflow of H^+ and more pronounced for lower exobase temperatures for the outflow of O^+. In the time-dependent study, it was found that the O^+ flux was negligible compared to the H^+ flux except at low altitudes characterized by high electron temperatures and high convection fields.

Nilsson et al. (2008) used data from the Composition and Distribution Function Analyzer (CODIF) to study the effect of centrifugal acceleration on outflows in the mantle region just poleward of the cusp. It was found that the centrifugal force caused acceleration in the range between 10 -100 m/s^2, which could cause a net energization of up to several hundreds of eV for O^+ ions. They also compared their results with a calculation of centrifugal acceleration based on the Tsyganenko T89 model (*Tsyganenko*, 1989) and found that there was an agreement at lower altitudes, but at high altitudes the modeled centrifugal acceleration increases as one over the square root of the magnetic field, while the observed centrifugal acceleration are several times higher than that. On the other hand, *Nilsson et al.* (2010) used combined Cluster Electric Field and Waves (EFW), Electron Drift Instrument (EDI), and Flux Gate Magnetometer (FGM) measurements to study the same effect on cold ion trajectories in the magnetotail lobes. They found that the centrifugal acceleration in the lobes was typically of the order of 1-10 m/s^2 , but when acting for long times it results in an increase of velocity of up to 20 km/s.

Nilsson et al. (2012) investigated the spatial variation of ion heating in the cusp, nightside polar cap, and central polar cap using Cluster measurements of ions and wave electric fields at high altitudes above the polar cap. They determined average flight trajectories above the

polar cap and focused on three distinct regions in particular: the cusp, the central polar cap, and the nightside polar cap. It was shown that the electric field spectral density at the O^+ gyrofrequency was mainly a function of altitude, while the efficiency in heating the ions seemed to be highest in the cusp at all altitudes. On the other hand, the efficiency was found to be much lower at altitudes below 7 R_E in the central and nightside polar cap. *Nilsson et al.* (2013) used Cluster observations of ion outflow (mainly O^+ outflow) and low-frequency waves above the polar cap to determine ion heating rates and low altitude boundary conditions that may be used in simulations of ion outflow. In their study they obtained expressions for the perpendicular velocity diffusion coefficients in the three regions defined by *Nilsson et al.* (2012). *Nilsson et al.* (2013) also observed that little or no heating in the altitude range of 5 to 7 R_E in the central and nightside polar cap would be consistent with the observations in those regions. The objective of our study is to investigate the properties of O^+ and H^+ outflowing ions and to emphasize the role of centrifugal acceleration on these properties by using a semikinetic model. This model includes the effects of the ambipolar electric field , wave-particle interaction, gravitational, mirror, and centrifugal forces. Three flux tubes, called central polar cap (CPC), nightside polar cap (NPC), and cusp, were taken to be along magnetic field lines calculated from Tsyganenko T96 model (*Tsyganenko*, 1995, 1996). The inclusion of wave-particle interaction is necessary to obtain a full picture of the energization process, and to discover any coupling between the centrifugal acceleration and wave-particle interaction. Furthermore the effect of centrifugal acceleration is simulated by considering three values of the ionospheric electric field; namely 0 (no centrifugal acceleration) , 50, and 100 mV/m.

Chapter 3

Model Description

This study is an extension of the problem considered by *Barghouthi* (2008) in the auroral oval and *Barghouthi et al.* (2011) in the polar cap with several modifications. These modifications include the magnetic field model, the flux tubes, the introduction of centrifugal acceleration, the perpendicular velocity diffusion coefficients and the initial conditions. The modifications will be described in chapter 3.1 and the direct simulation Monte Carlo (DSMC) method used will be briefly described in chapter 3.2.

3.1 Model Modifications

3.1.1 Magnetic Field Model and Flight Trajectories

The first modification is the replacement of the radial magnetic field with a magnetic field calculated from Tsyganenko T96 model with the solar ram pressure set to 3.28 nPa, the DST-index to -6, and the y- and z-components of the interplanetary magnetic field to 5.84 and -6.3 nT respectively (*Zhang et al.*, 2008). Figure 3.1 shows the calculated magnetic field lines in solid black and blue lines separated by 5° in latitude at the surface of the earth. A model magnetopause is shown by a red dotted line. It may be clearly seen that at altitudes above about 10 R_E the magnetic field can no longer be assumed to be radial and the curvature

of the magnetic field is significant.

In this study we will consider ion outflow along three main trajectories proposed by *Nilsson et al.* (2012). In Figure 3.1 they are shown by thick blue lines. The most sunward blue line will represent the flux tube that we will call the cusp. The most poleward blue line will represent the flux tube that will be called nightside polar cap (NPC) . The central blue line will be called the central polar cap (CPC). The flux tube we call cusp is not to be confused with the mid-altitude equatorward edge of the cusp studied by *Bouhram et al.* (2004).

3.1.2 Centrifugal Acceleration

As is shown in equation 1.12, the electric field and the directional derivatives of the magnetic fields are needed to evaluate the centrifugal acceleration. The directional derivatives of the magnetic field were obtained using Tsyganenko T96 model while the electric field was calculated using the convection electric field model suggested by *Cladis* (1986) which was calculated for open field lines along the noon-midnight meridional plane and points from dawn to dusk. The expression for the convection electric field is given by:

$$E = E_i \sqrt{\frac{B}{B_i}} \tag{3.1}$$

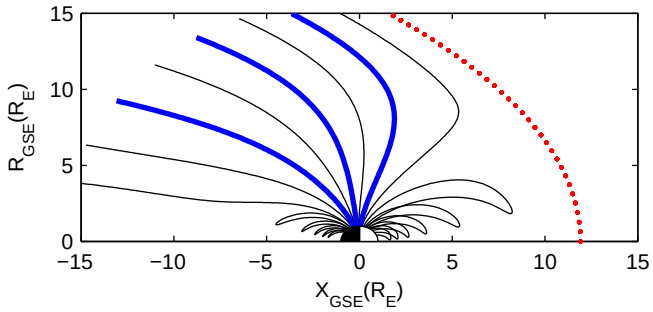

Figure 3.1: Magnetic field lines from Tsyganenko T96 model. Solid black and blue lines represent sample field lines spaced 5° apart. Solid blue lines indicated the trajectories of ions in the three regions considered in this study. A model magnetopause is indicated by a red dotted line.

where E_i and B_i are the electric field and magnetic field intensities at the surface of the ionosphere and were assumed to be constant within the polar cap and E is the electric field when the magnitude of the magnetic intensity is B .

Figure 3.2 shows the perpendicular and partial parallel term of centrifugal acceleration (CA). Solid and dashed black lines represent the calculation of *Horwitz et al.* (1994) along a line of latitude 90° for ionospheric electric fields of 50 and 100 mV/m respectively. Solid black triangles represent the calculations of *Nilsson et al.* (2008) based on observations for the magnetic and electric fields measured on board the cluster spacecraft in the dayside region of the polar cap. Blue and red lines represent our calculations for E_i = 50 and 100 mV/m respectively. Solid lines represent the CPC, dotted lines represent the cusp, and dashed lines represent the NPC. In our study the effect of centrifugal acceleration is studied through considering three values of E_i = 0 (no centrifugal acceleration) , 50, and 100 mV/m.

As shown in Figure 3.2 the parallel term is extremely significant in the centrifugal acceleration and cannot be ignored as suggested by *Horwitz et al.* (1994) even for the central polar cap. The calculations for the perpendicular term differ by a factor of about 6, this has to do with the fact that we calculate the derivatives along a field line while *Nilsson et al.* (2008) calculated these values at given altitudes for locations where the four-spacecraft were not in the same plane and these are not necessarily representative of a given flight trajectory.

3.1.3 Perpendicular Velocity Diffusion Coefficients

The diffusion coefficients considered in this paper were obtained from a combination of several studies. For O^+ ions in CPC, NPC, and cusp at lower altitudes (<3.7 R_E) the diffusion coefficients calculated by *Barghouthi et al.* (1998) in the polar wind were used. These diffusion coefficients were calculated from spectral densities measured by the Plasma Wave Instrument on board the Dynamics Explorer-1 (DE-1) spacecraft. This data spanned a range of altitudes from 1.5 to 4.5 R_E. In the mid altitude region (between 3.7 and 7.5 R_E) of the CPC and NPC the diffusion coefficients were set to zero to simulate a no wave-particle

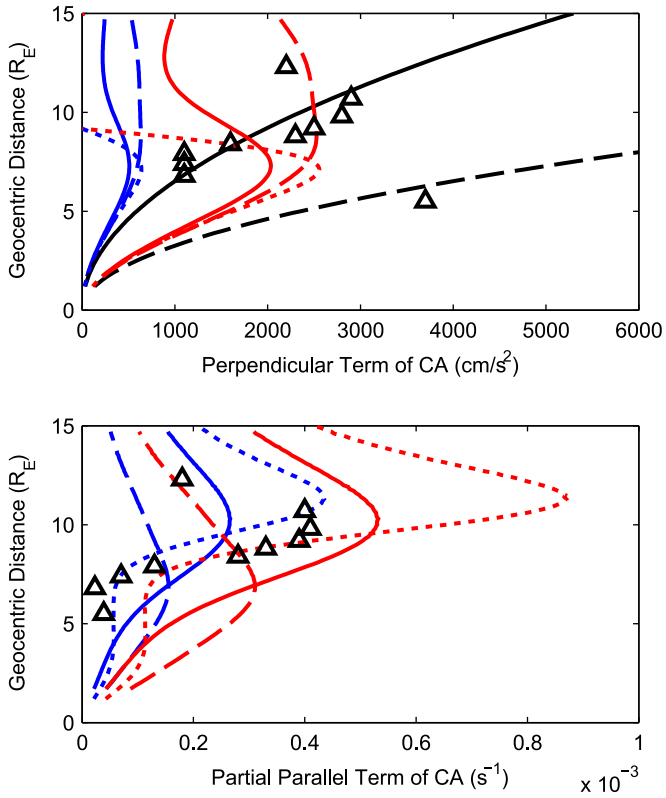

Figure 3.2: Perpendicular term (top panel) and partial parallel term (bottom panel) of centrifugal acceleration (CA). Solid and dashed black lines represent the centrifugal acceleration calculated by *Horwitz et al.* (1994) for E_i= 50, 100 mV/m respectively. Triangles represent the calculations of *Nilsson et al.* (2008) based on observations. Blue and red lines represent our calculations for E_i= 50, 100 mV/m respectively. The CPC is represented by solid blue and red lines, the NPC by dashed blue and red lines, and the cusp by dotted blue and red lines.

interaction region suggested by the measurements of parallel velocities and perpendicular temperatures presented by *Nilsson et al.* (2012, 2013) (see Figure 3.3). At higher altitudes (>7.5 R_E) in the CPC and NPC the diffusion coefficients calculated by *Nilsson et al.* (2013) were used. These diffusion coefficients were calculated based on data at altitudes higher than 7 R_E collected from the Electric Field and Wave Instrument on board the Cluster spacecraft. In the cusp region at altitudes higher than 3.7 R_E, the diffusion coefficients presented by *Nilsson et al.* (2013) were used for all altitudes. The coefficients calculated by *Barghouthi* (1997) in the auroral region were not used for the cusp at lower altitudes (< 3.7 R_E) since they are representative of the equatorward edge of the cusp and are much too high to be representative of the cusp region considered in this study. For hydrogen ions the diffusion coefficients calculated by *Nilsson et al.* (2013) were used for all altitudes and all regions.

The diffusion coefficients were chosen such that the parallel bulk velocities and perpendicular temperatures fit the observations made by *Nilsson et al.* (2013). To illustrate this we show the parallel bulk velocities and perpendicular temperatures for O^+ ions in the central polar cap in Figure 3.3. Red circles with error bars show the observed values based on Cluster CODIF data reported by *Nilsson et al.* (2013). Error bars indicate 95% confidence. We studied three different combinations of diffusion coefficients. First we used the diffusion coefficients of *Nilsson et al.* (2013) for all altitudes. The results are shown using blue lines and denoted by 'N'. Second we used the diffusion coefficients proposed by *Barghouthi et al.* (1998) up to 4 R_E and the diffusion coefficients of *Nilsson et al.* (2013) above 4 R_E. The results are shown by green lines and are denoted 'BN'. Finally we considered the *Barghouthi et al.* (1998) diffusion coefficients up to 3.7 R_E, no WPI between 3.7 and 7.5 R_E, and *Nilsson et al.* (2013) diffusion coefficients above 7.5 R_E. The results are shown by black lines and are denoted by 'BWN'. Clearly the third case best fits the observations and thus this choice was adopted for the rest of the study.

A similar procedure was used for the NPC and cusp to chose the best diffusion coefficients. The drop of perpendicular temperature between 5 and 7 R_E may indicate the presence of no or little heating in that region of the CPC and NPC. Although the wave activity is present at

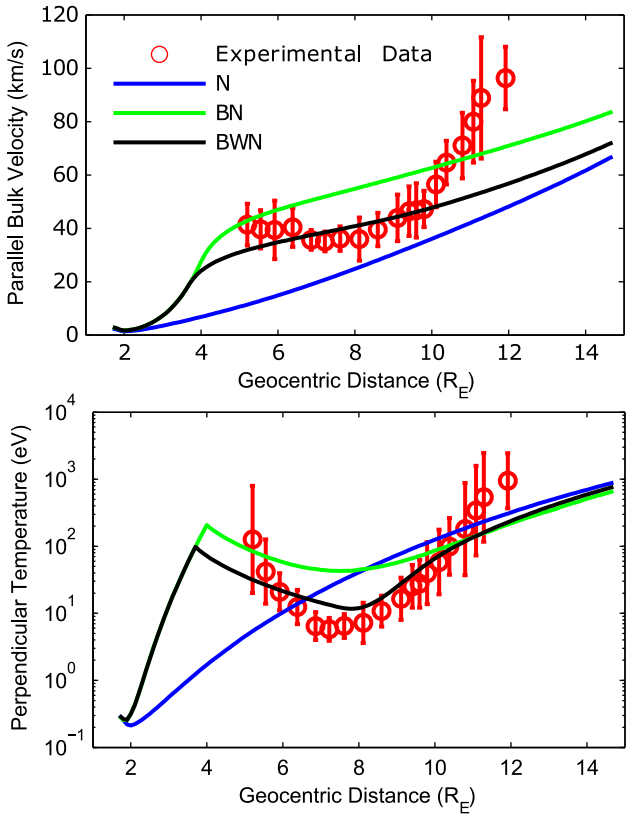

Figure 3.3: Profiles of parallel bulk velocity (top panel) and perpendicular temperature (bottom panel) for O^+ ions in the CPC. Red circles with error bars represent observations based on Cluster CODIF data from the high altitude polar cap reported by *Nilsson et al.* (2013). Error bars indicate 95% confidence. Solid lines represent model results for different diffusion coefficient combinations.

Table 3.1: Perpendicular velocity diffusion coefficients used in this study. Diffusion coefficients are in units of cm^2/s^3, and in r is in units of R_E

		$r < 3.7\ R_E$	$r \in [3.7,7.5] R_E$	$r > 7.5\ R_E$
O^+	CPC	$9.55 \times 10^2 r^{13.3}$	0	$\eta 1 \times 10^5 r^{5.5}$
	NPC	$9.55 \times 10^2 r^{13.3}$	0	$\eta 1.725 \times 10^7 r^{3.3}$
	Cusp	$9.55 \times 10^2 r^{13.3}$	$\eta 5 \times 10^4 r^{6.4}$	
H^+	All Regions	$\eta 2.3 \times 10^{10}$		

all altitudes in all regions the fraction of this wave activity that is efficient in heating the ions is much smaller in the CPC and NPC in mid altitudes and it is reasonable to assume that there is no wave-particle interaction in this region. This is not the case in the cusp region where the fraction η is much higher. Another possible explanation that will not be pursued in this research, is the existence of a cooling mechanism in this region, other than adiabatic cooling.

Table 1 shows the expressions for the diffusion coefficients that have been used in this study in the three regions and at different altitudes. In Table 1, r is the geocentric distance in units of earth radii (R_E), and η is the fraction of spectral density at the ion gyrofrequency that is efficient in heating as was introduced in chapter 2. The fraction η is already absorbed in the diffusion coefficients given by *Barghouthi et al.* (1998), however *Nilsson et al.* (2013) left it as a fitting parameter. Whenever using *Nilsson et al.* (2013) diffusion coefficients we will set $\eta = \frac{1}{2}$ for the CPC and cusp and $\eta = \frac{1}{15}$ for the NPC. Therefore in the CPC and NPC we are explicitly setting $\eta = 0$ for the mid altitude region (between 3.7 and 7.5 R_E).

3.1.4 Boundary Conditions

O^+ ions at the lower altitude boundary were assumed to have a density and drift velocity of 10 cm^{-3} and 2 km/s respectively for the CPC and NPC and 10000 cm^{-3} and 0.5 km/s respectively for the cusp as suggested by *Nilsson et al.* (2013). H^+ ions at the lower altitude boundary were assumed to have a density and drift velocity of 34 cm^{-3} and 18 km/s respectively for the CPC and NPC as suggested by *Nilsson et al.* (2013) and 200 cm^{-3} and 16 km/s respectively

for the cusp as in *Barghouthi* (1997). Finally the simulation tube was extended to a large range of altitudes, namely from 1.7 R_E to 14.7 R_E in the CPC and NPC, and from 1.2 R_E to 15.2 R_E in the cusp. The temperature at the exobase was assumed to be 3000 K for both ions and electrons in all regions .

3.2 DSMC Method

A Monte Carlo simulation was used to study the outflow of ions under the effect of WPI, centrifugal acceleration, body forces and diverging magnetic field lines in the three regions described above. The ions were injected at the exobase (r_0= 1.7 R_E for the CPC and NPC and r_0= 1.2 R_E for the cusp) with a velocity consistent with the ion distribution function. The ion motion was followed for a small time interval $\triangle t$ as it moves under the influence of the body forces, centrifugal acceleration and mirror force. The influence of WPI during this time interval is simulated by incrementing the ion's perpendicular velocity by a random increment $\triangle v_\perp$ that satisfies:

$$< (\triangle v_\perp)^2 >= 4 D_\perp \triangle t \tag{3.2}$$

The simulation tube is divided into bins (140 bins for the cusp and 130 bins for the CPC and NPC) which act as registrars. As the ion crosses one of these registrars, it's parallel and perpendicular velocity are registered for later use. A large number of ions (10^5-10^7) are followed until they either exit from the top of the tube (at 14.7 R_E for the CPC and NPC and at 15.2 R_E for the cusp) or from the bottom. At the end of the simulation the registered data is used to calculate the ion moments and the distribution functions at the designated altitudes. For a more detailed description on the method and how the moments and distribution functions are calculated see *Barghouthi et al.* (2003).

The initial distribution function from which the initial velocities were generated was assumed to be a drifting Maxwellian. Since the electrostatic potential depends on the density

and the centrifugal acceleration depends on the parallel velocity, which are actually outputs of the simulation, an iterative approach was conducted. The electrostatic potential and centrifugal acceleration are calculated initially with an approximate profile for the density and velocity. These approximated values are used to run the simulation. At the end of the simulation the output values of density and velocity are used to calculate new profiles for the centrifugal acceleration and potential which are used to run the simulation again. These steps are repeated until convergence is reached which is typically within three to four runs, after which the final values of moments and distribution function are extracted.

Chapter 4

Results

In this study we present our results for different values of E_i = 0 (no centrifugal acceleration), 50 and 100 mV/m for the three regions. Accordingly, this chapter will be divided into three subsections, one for each region. For each region we present the moment profiles for O^+ and H^+ ions. We also present the distribution functions for the O^+ ions. The behavior of the distribution functions for H^+ ions is discussed without displaying them.

4.1 Central Polar Cap (CPC)

Figure 4.1 and 4.2 show the density, parallel bulk velocity, perpendicular temperature, and parallel temperature for O^+ (Figure 4.1) and H^+ (Figure 4.2) ions. Clearly centrifugal acceleration has little or no effect on the density of O^+ ions, however it has the effect of lowering the density of H^+ ions at higher altitudes. The density of O^+ ions is negligible with respect to H^+ ions at high altitudes. For example at a geocentric distance of 5 R_E the density of O^+ and H^+ ions are about 0.006 and 0.65 cm^{-3} respectively.

The effect of centrifugal acceleration is much more evident in the significant increase of parallel bulk velocity for both O^+ and H^+ ions at altitudes above about 4 R_E. At 10 R_E, the O^+ parallel bulk velocity increases from about 38 km/s for no centrifugal acceleration to 48 km/s and 63 km/s for E_i= 50 and 100 mV/m respectively. In contrast the H^+ velocity increases

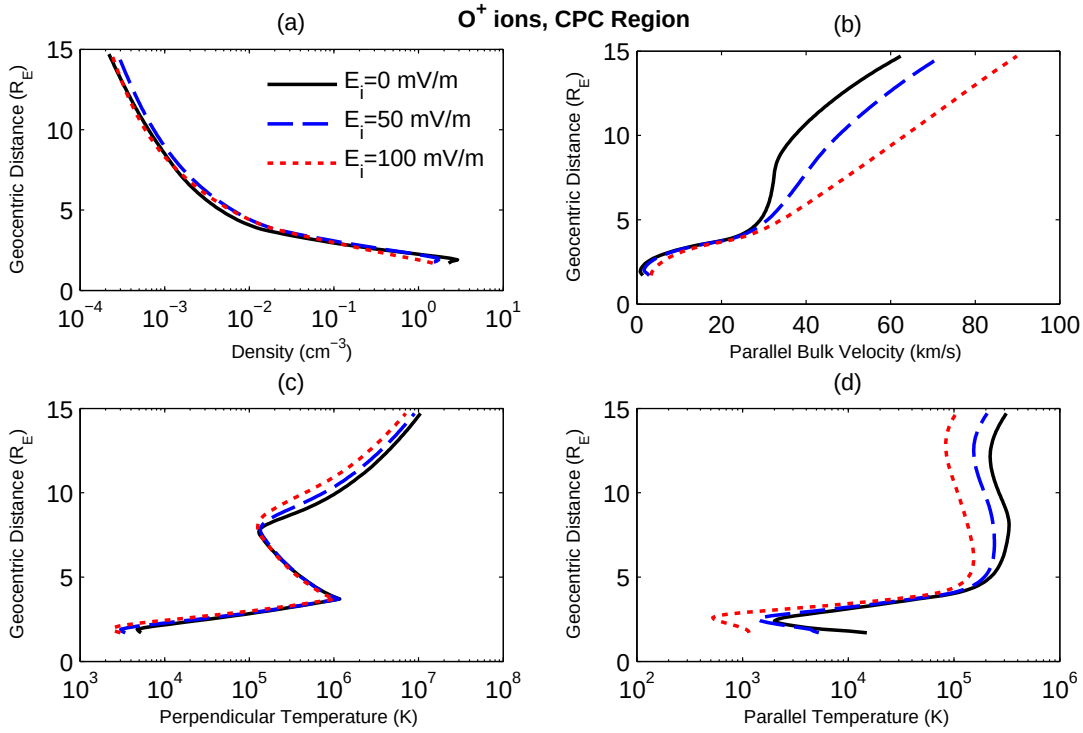

Figure 4.1: O^+ (a) density (b) parallel bulk velocity (c) perpendicular temperature and (d) parallel temperature profiles in the central polar cap region.

from 52 km/s for E_i= 0 mV/m to 61 km/s and 76 km/s for E_i= 50 and 100 mV/m respectively.

Both parallel and perpendicular temperatures tend to decrease with increasing ionospheric electric fields above about 4 R_E, but the decrease is more substantial in the parallel temperature. At 14.7 R_E the parallel and perpendicular temperatures of H^+ ions were decreased from about 1.1×10^4 and 8.7×10^4 K respectively to about 4.1×10^3 and 6.1×10^4 K respectively when E_i was increased from 0 to 100 mV/m. At the same altitude the parallel and perpendicular temperatures of O^+ ions were decreased from about 3.1×10^5 and 1.1×10^7 K respectively to about 1.0×10^5 and 7.0×10^6 K respectively when E_i is increased from 0 to 100 mV/m. Thus centrifugal acceleration clearly leads to higher temperature anisotropy. For example the perpendicular to parallel temperature ratio of O^+ ions at 13 R_E is about 24, 29, and 40 for E_i =0, 50, 100 mV/m respectively. For H^+ ions the ratio at the same altitude is about 7, 10, and 13 for E_i =0, 50, 100 mV/m respectively. Another expected feature is the rapid decrease of perpendicular temperature for O^+ ions between 3.7 and 7.5 R_E due to the absence of WPI in this region and the presence of perpendicular adiabatic cooling.

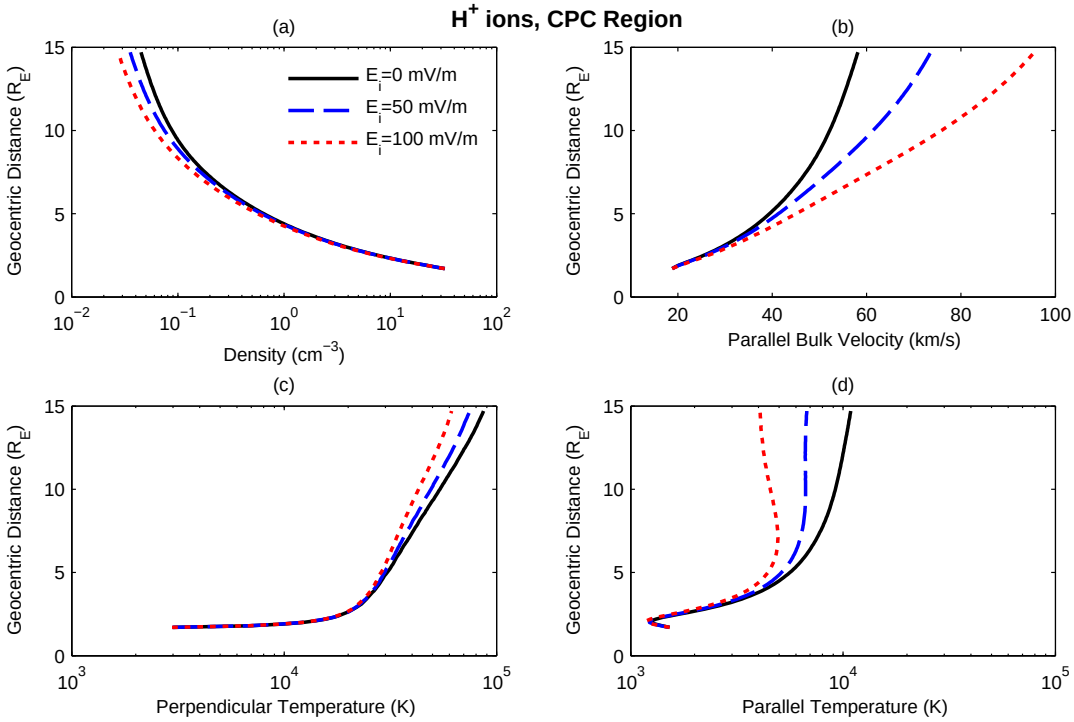

Figure 4.2: H^+ (a) density (b) parallel bulk velocity (c) perpendicular temperature and (d) parallel temperature profiles in the central polar cap region.

Figure 4.3 shows the O^+ ion velocity distributions in the CPC (first two columns), NPC (3rd and 4th columns), and cusp (5th and 6th columns) for E_i=0, and 50 mV/m. The distribution functions of O^+ ions exhibit an interesting behavior since the diffusion coefficients differ at different altitudes. In the first altitude range (from 1.7-3.7 R_E) the distribution functions quickly develop a conic shape due to strong WPI. In the mid altitude region (3.7-7.5 R_E) the distribution functions shrink in the perpendicular direction and grow in the parallel direction due to the effect of the mirror force and the absence of WPI. At high altitudes (>7.5 R_E) the distribution functions return to form conic distributions. It is noticed however that O^+ ions saturate at conic distributions much slower in the high altitude region and this may be contributed to the much smaller diffusion coefficients in this region (see Table 1). As E_i is increased from 0 to 50 mV/m the distribution functions become narrower in the parallel direction as a consequence of the increase of parallel bulk velocity which reduces the dispersion of the parallel velocities. This is further evidence for the effect of centrifugal acceleration on temperature anisotropy. The velocity distribution of H^+ ions (not shown here) form conic features at 3.5 R_E and saturate at these distributions for all altitudes.

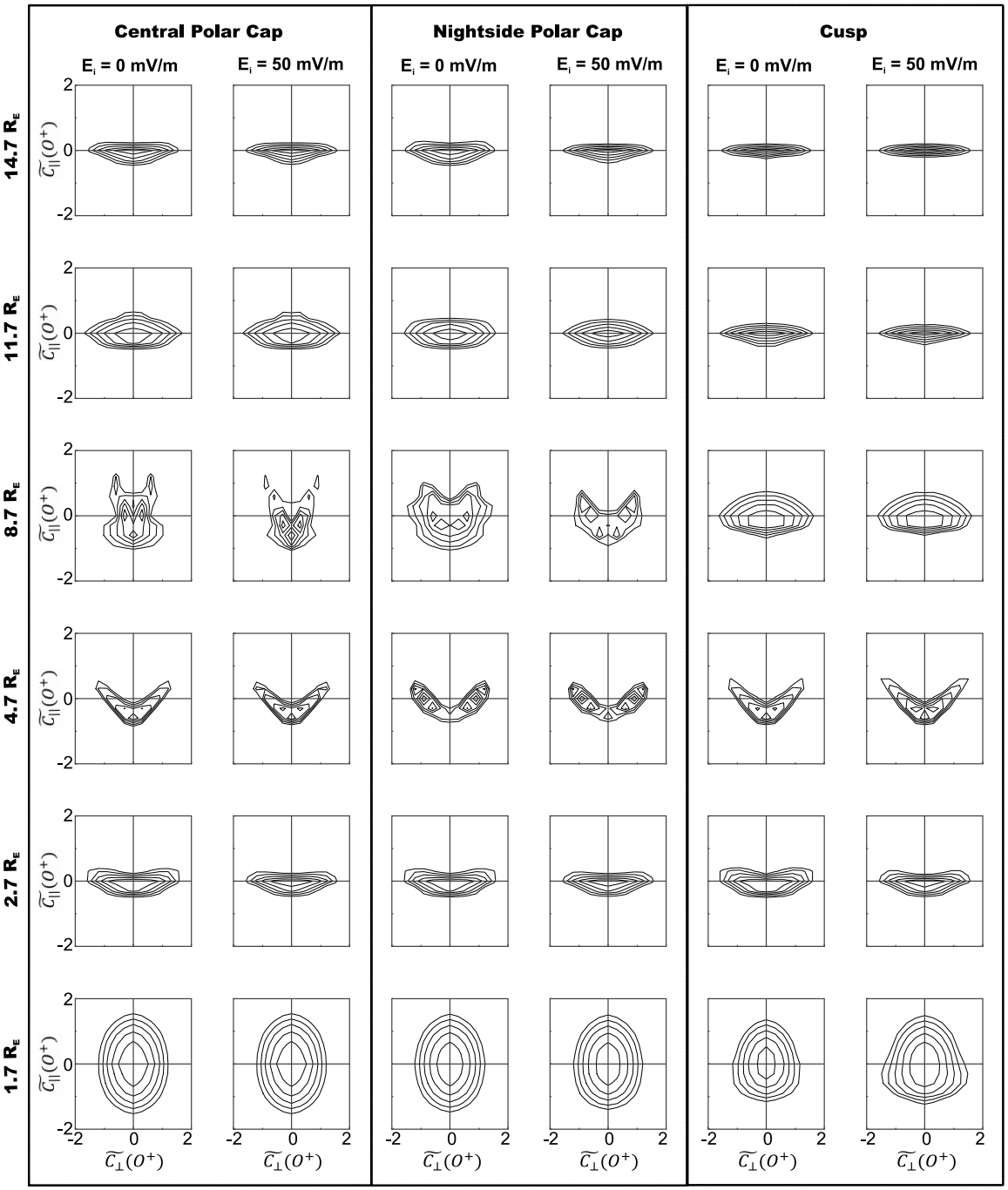

Figure 4.3: O^+ion velocity distributions in the CPC (first two columns), NPC (3rd and 4th columns), and cusp (5th and 6th columns) for E_i=0, and 50 mV/m at 1.7, 2.7, 4.7, 8.7,11.7, and 14.7 R_E, where $\tilde{C} = (v - \mathbf{u})/\sqrt{2kT/m}$. The contours decrease successively by a factor of $e^{0.5}$ from the maximum.

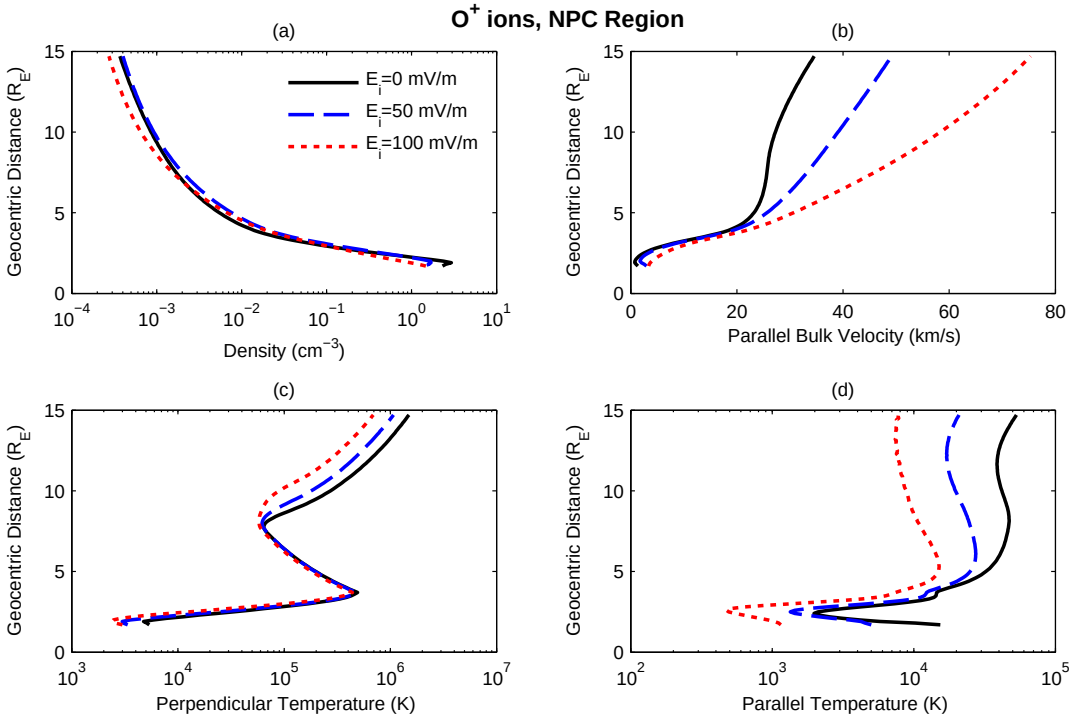

Figure 4.4: O^+ (a) density (b) parallel bulk velocity (c) perpendicular temperature and (d) parallel temperature profiles in the nightside polar cap region.

4.2 Nightside Polar Cap (NPC)

Figure 4.4 and 4.5 show the velocity moments for O^+ and H^+ ions respectively in the nightside polar cap region. Centrifugal acceleration has little or no effect on the density of O^+ ions, and decreases the H^+ ion density. In the nightside polar cap it is also true that the density of O^+ ions is negligible compared to H^+ ions at high altitudes. For example at 8 R_E the density of O^+ and H^+ ions for E_i = 50 mV/m is about 1.7×10^{-3} and 0.12 cm^{-3}.

As expected increasing ionospheric electric fields have the effect of significantly increasing the parallel bulk velocity for both ions. At 10 R_E the parallel bulk velocity of O^+ ions increases from about 27 km/s when no centrifugal acceleration was present to nearly 39 and 58 km/s for E_i = 50 and 100 mV/m respectively. For H^+ ions at the same altitude the parallel bulk velocity increases from about 34 km/s for E_i = 0 mV/m to 46 and 65 km/s for E_i = 50 and 100 mV/m respectively. It may be noticed that increasing the ionospheric electric field from 0 to 50 mV/m has the effect of increasing the parallel bulk velocity by approximately 12 km/s for both ions. While when the ionospheric electric field is increased from 50 to 100

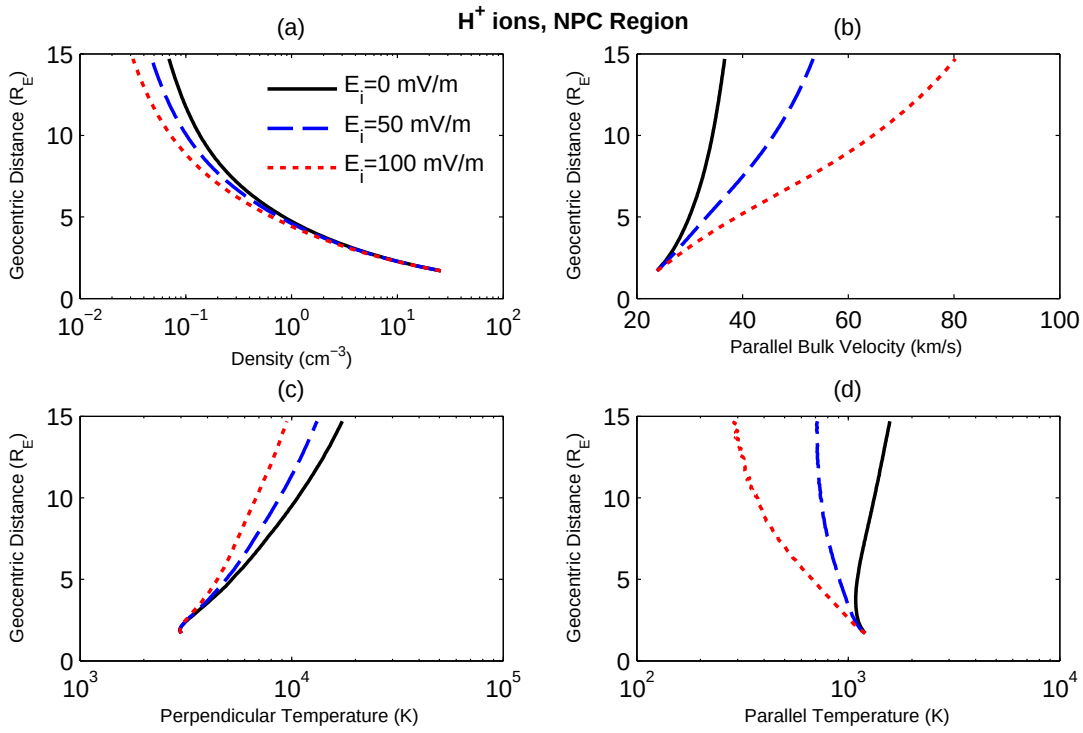

Figure 4.5: H^+ (a) density (b) parallel bulk velocity (c) perpendicular temperature and (d) parallel temperature profiles in the nightside polar cap region.

mV/m the parallel bulk velocity was increased by about 19 km/s for both ions. This pattern is not trivial since centrifugal acceleration does include a species dependent term through the parallel velocity (see equation 1.12). The implications made by this pattern will be discussed in more detail in chapter 5. There is however a difference between the parallel bulk velocity profile of both ions at lower altitudes. The increase of E_i affects H^+ ions from the beginning of the flux tube, while increasing E_i only affects the parallel bulk velocity of O^+ ions above about 4 R_E.

The significant increase in parallel bulk velocity is accompanied by a significant decrease in the parallel temperatures of both species with increasing E_i. Again like the parallel bulk velocity the parallel temperature of H^+ ions begins to be affected by increasing E_i at the lowest altitudes while the parallel temperature of O^+ ions is significantly affected after about 4 R_E. The perpendicular temperature of H^+ ions increased slowly with altitude with a change of only one order of magnitude between the lowest and highest altitudes. Increasing the centrifugal acceleration has the effect of lowering the perpendicular temperature at a given altitude. The

effect however is not as pronounced as in the parallel temperature which leads to higher temperature anisotropy. To illustrate, at the highest altitudes the perpendicular to parallel temperature ratios for H^+ ions were 11, 18, and 33 for E_i = 0, 50, and 100 mV/m respectively. The perpendicular temperature of O^+ ions increases by more than two orders of magnitude between 1.7 and 3.7 R_E due to high WPI. In the mid altitude region (between 3.7 and 7.5 R_E) the perpendicular temperature decreases rapidly due to adiabatic cooling and the absence of WPI. At altitudes higher than 7.5 R_E the perpendicular temperature increases , but much slower than it did in the low altitude region due to much lower velocity diffusion coefficients (see Table 1). The effect of centrifugal acceleration on the perpendicular temperature is negligible below 7.5 R_E. Above this altitude perpendicular temperatures decrease with increasing E_i at a given altitude . The perpendicular to parallel temperature ratio for O^+ ions at 14.7 R_E is 28, 51, and 89 for E_i= 0, 50, and 100 mV/m respectively.

The distribution functions for O^+ ions quickly saturate into conic shapes below 3.7 R_E. Between 3.7 and 7.5 R_E the absence of WPI becomes evident as the mirror force causes the distribution function to shrink in the perpendicular direction and elongate in the parallel direction. At high altitudes the conic distributions reform. With increasing centrifugal acceleration the distribution functions become narrower in the parallel direction, which indicates less dispersion of parallel velocities, or in other words smaller parallel temperatures. Distribution functions for H^+ ions (not shown here) develop slowly into conic distributions, which are clearly seen above about 7.7 R_E. This is an indication of weak WPI in this region.

4.3 Cusp

Figure 4.6 and 4.7 show the velocity moments for O^+ and H^+ ions respectively for the cusp region. The density profiles of both O^+ and H^+ ions decrease as a function of altitude, however the density of O^+ ions is at least one order of magnitude less than that of the H^+ ions. For example the ratio of the density of O^+ ions to the density of H^+ ions for E_i= 50 mV/m is about 4.0×10^{-2} and 3.0×10^{-2} at altitudes of 5 and 10 R_E respectively. As in

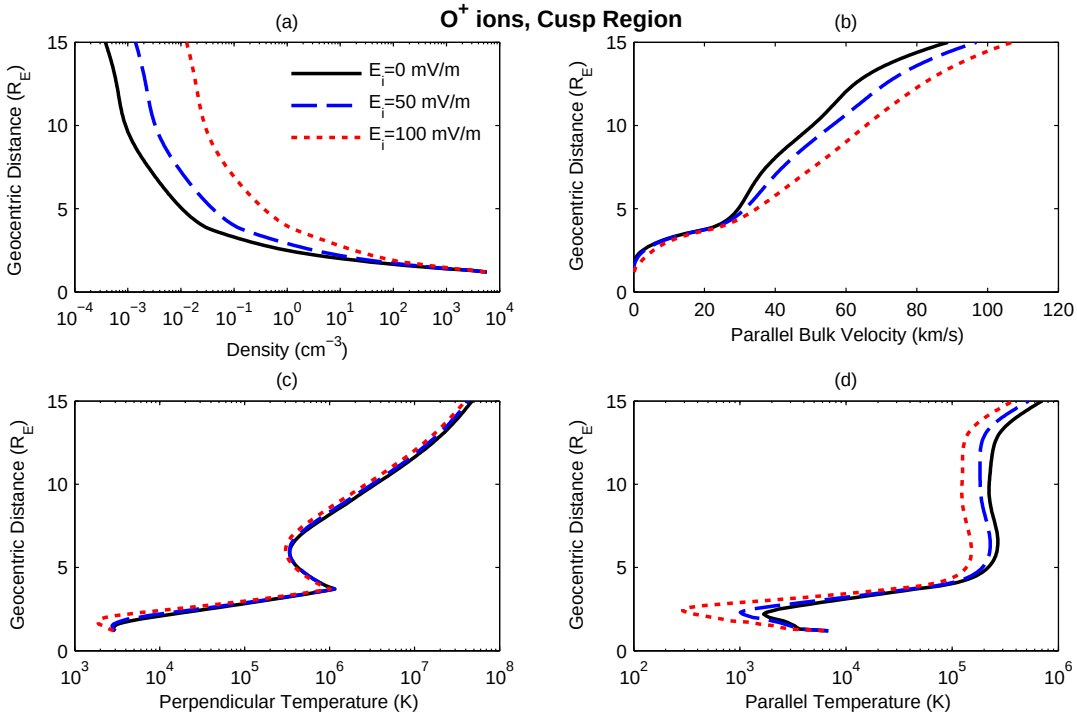

Figure 4.6: O^+ (a) density (b) parallel bulk velocity (c) perpendicular temperature and (d) parallel temperature profiles in the cusp region.

the previous two regions, the density of H^+ ions decreases slightly with increasing E_i. This is not the case for O^+ ions, however , as increasing the ionospheric electric fields has the effect of significantly increasing the density at high altitudes. For example, the density of O^+ ions at 10 R_E is 9.1×10^{-4}, 3.3×10^{-3}, and 2.8×10^{-2} cm^{-3} for E_i= 0, 50, and 100 mV/m respectively.

The parallel bulk velocity of both ions increase significantly with increasing E_i. For example at 10 R_E the parallel bulk velocity of O^+ ions increases from about 51 km/s at E_i=0 mV/m to 56 km/s and 66 km/s for E_i = 50 and 100 mV/m respectively. While for H^+ ions the increase was from 55 km/s at E_i=0 mV/m to 62 km/s and 74 km/s for E_i = 50 and 100 mV/m respectively. Thus it is evident from these values and from Figures 4.6 and 4.7 that the increase in bulk velocities is not the same for both ions. At 3.7 R_E, the perpendicular temperature of O^+ ions suddenly begins to decrease with altitude due to the sudden change of diffusion coefficients at that altitude. The perpendicular temperature returns to increase with altitude above about 6 R_E. The parallel temperature for both ions decreases at a given altitude with increasing E_i. However, the effect of increasing centrifugal acceleration on

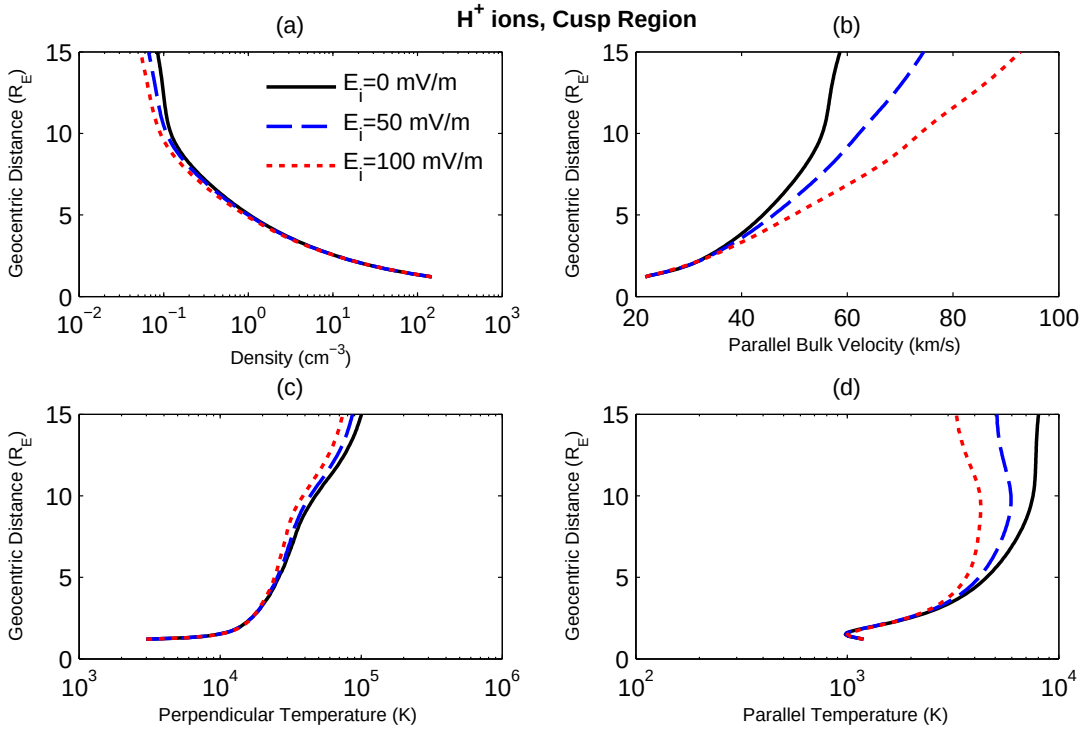

Figure 4.7: H^+ (a) density (b) parallel bulk velocity (c) perpendicular temperature and (d) parallel temperature profiles in the cusp region.

perpendicular temperature is very small, and therefore the anisotropy increases when E_i is increased. For example the perpendicular to parallel temperature ratio of O^+ ions at 14 R_E is 82, 101, and 130 for E_i= 0, 50, and 100 mV/m respectively, while this ratio for H^+ ions at the same altitude is 12, 16, and 21 for E_i= 0, 50, and 100 mV/m respectively.

O^+ ion distribution functions saturate into conic distributions very early as in the other two regions. Between 3.7 and 6.0 R_E the distribution functions exhibit a deviation from the conic distributions to a distribution elongated more in the parallel direction. The effect of centrifugal acceleration in this region is to reduce the distribution in the parallel direction. H^+ ion distribution functions (not shown here) saturate into conic distributions early and do not change for the rest of the flux tube.

Chapter 5

Discussion

It is evident that in all regions the density of O^+ ions is much less than that of H^+ ions at high altitudes and that the profiles of both ion species are monotonically decreasing with altitude. At E_i= 50 mV/m the density of O^+ ions in the cusp is about one order of magnitude larger than in the CPC and NPC regions at the top of the flux tube. The density of H^+ ions at a given value of E_i are of the same order of magnitude for all three regions. The general behavior of H^+ density is to decrease with increasing E_i at a given altitude. This is well understood due to the fact that all ions already have sufficient energy to overcome the potential barrier, and therefore an increase of centrifugal acceleration leads to an increase of parallel bulk velocity. Since there is no sources of ions on the trajectory and no more ions can be injected at the exobase the flux of ions must be conserved. This condition implies that an increase of the parallel bulk velocity yields a decrease of the corresponding density. The behavior of the O^+ density profiles with increasing centrifugal acceleration is less trivial. The effect depends on how much ions escape the potential barrier without the influence of centrifugal acceleration. In the cusp the density increases with increasing E_i. This increase in density is a clear indication that centrifugal acceleration actually causes more ions to be able to overcome the potential barrier. The density is affected more in the cusp with increasing ionospheric electric fields due to two reasons: the higher terms of centrifugal acceleration and the higher density and lower velocity of O^+ ions at the exobase. In the CPC and NPC

the density of O^+ ions is unaffected by the centrifugal acceleration. Therefore the effect of increasing upflow ions and the decrease of density due to increasing velocity cancel each other.

There is a direct coupling between increasing velocities and decreasing parallel temperatures and therefore we will focus for now on the bulk velocities. The bulk velocities were the highest in the cusp followed by the CPC and the NPC. This can be understood when considering the relative strength of the WPI in the three regions (see Table 1). These results clearly indicate that WPI is strongest in the most sunward portion of the polar cap.

It was noted in chapter 4.2 that when increasing the ionospheric electric field by a given amount the bulk velocities for both ions increase by the same amount. In the CPC and NPC at 10 R_E the parallel bulk velocity increased by about 10 and 12 km/s respectively for both ion species when going from E_i = 0 to 50 mV/m. On the other hand, when going from E_i = 50 to 100 km/s the increase was about 15 and 19 km/s for both ion species in the CPC and NPC respectively. This is odd since the centrifugal acceleration does depend on the particular species in consideration through the parallel velocity (see equation 1.12). Why do O^+ and H^+ ions appear to be accelerated by the same amount even though they have significantly different velocity profiles? The answer is simple; when a particle has a high velocity, the time it spends being accelerated is less than a slower particle. On the other hand, since the parallel term of centrifugal acceleration is linearly dependent on the velocity, faster particles will experience a higher acceleration. In most cases these two effects cancel out and the total centrifugal acceleration appears to be species independent. This effect is discussed by *Nilsson et al.* (2010). In addition, the increase of parallel bulk velocity is not the same when going from E_i = 0 to 50 mV/m and when going from E_i = 50 to 100 mV/m even though the increase in E_i is the same in both cases. This may be comprehended in view of equation 1.12, in which it is noticed that the perpendicular term of the centrifugal acceleration has a quadrature term in $\mathbf{V_E}$. There are exceptions however, such as the O^+ ions in the cusp. In the cusp there is no relation between the increase of O^+ and H^+ parallel bulk velocity (see Figures 4.6 and 4.7). This is due to the high diffusion coefficients of O^+ ions in comparison

to the H^+ diffusion coefficients in the cusp. In particular the diffusion coefficients of O^+ ions are two orders of magnitude larger than those of H^+ ions at high altitudes. The difference in the CPC and NPC is only only of one order of magnitude at high altitudes.

Moreover it was noticed that the effect of centrifugal acceleration on bulk velocities only show above about 4 R_E . This may be explained due to the lower centrifugal acceleration terms (see Figure 3.2) and lower velocities at lower altitudes. H^+ ions in the NPC show an early response to centrifugal acceleration (see chapter 4.2). This rises the main question: why isn't this effect seen in other regions for H^+ ions? To answer this question we refer to Figure 3.2b where it should be noticed that the partial parallel term in the NPC is larger than in the other two regions. Hence, although the initial velocity at the exobase is practically the same for all three regions, the centrifugal acceleration experienced by H^+ ions in the NPC is much higher. O^+ ions do not feel the effect of centrifugal acceleration at the lower altitudes due to their low velocities and the fact that the perpendicular term of the centrifugal acceleration (which is velocity independent) is very small.

As noted above, at a given altitude if the parallel bulk velocity of an ion species increases its parallel temperature decreases. This effect is called parallel adiabatic cooling (see *Barghouthi et al.*, 1993) and states that if an ion is accelerated in the parallel direction, the dispersion of velocities should decrease, leading to lower parallel temperatures. The perpendicular temperatures also decrease with increasing centrifugal acceleration at a given altitude. Although there is no direct coupling between the parallel bulk velocity and perpendicular temperature, increasing the parallel bulk velocity of an ion causes it to spend less time in a given region of WPI and therefore it is heated less in the transverse direction. This causes the perpendicular temperature to fall with increasing ionospheric electric fields at a given altitude. This explanation may be verified by noticing that the perpendicular temperature was not changed with respect to E_i in the region of no WPI (between 3.7 and 7.5 R_E in the CPC and NPC) when E_i was increased, even though the parallel velocity was significantly increased with enhanced E_i in this region (see Figures 4.1 and 4.4). This is a clear indication that the centrifugal acceleration only affects the perpendicular temperature in the presence of WPI. The parallel

temperature is affected much more than the perpendicular temperature with increasing centrifugal acceleration, which leads to much higher temperature anisotropies. The anisotropy was higher for O^+ ions than for H^+ ions and it was the highest in the cusp.

The general behavior of the perpendicular temperature profiles was to increase with altitude in regions of strong WPI. Thus it may be seen that in the cusp the increase of O^+ perpendicular temperature was the highest. At lower altitudes for all three regions (which have much larger diffusion coefficients) a rapid increase in perpendicular temperature is seen, while the mid altitude region experiences a rapid decrease of perpendicular temperature due to perpendicular adiabatic cooling which imitates the behavior described by *Nilsson et al.* (2013) in these regions. In the cusp, at mid altitudes (between 3.7 and 6.0 R_E) the perpendicular temperature falls off even in the presence of WPI. This may be attributed to the large jump in the diffusion coefficients at 3.7 R_E. The mirror force is proportional to the perpendicular velocity, therefore when the diffusion coefficients were changed at 3.7 R_E the perpendicular temperature was high, leading to high adiabatic cooling, while the diffusion coefficients are low and therefore the mirror force overcomes WPI and the perpendicular temperature falls with altitude. This continues until the perpendicular temperature is low enough for the mirror force and WPI to be comparable. At high altitudes, the perpendicular temperature increases slower than the low altitude region due to the weaker WPI in this region. Additionally, the H^+ perpendicular temperature increases approximately at the same rate with altitude in the CPC and cusp and slightly slower in the NPC. This is because of the equal diffusion coefficients in the CPC and cusp and the smaller diffusion coefficients in the NPC for H^+ ions due to lower η.

The distribution functions tend to form conic distributions in the regions of considerable WPI. It was noticed that the conic distribution form much faster in regions with high diffusion coefficients. The formation of conic distributions is due to the combined effect of WPI and the mirror force. WPI heats the ions in the perpendicular direction and the mirror force converts part of the perpendicular energy into the parallel direction, thus forming conic distributions. In regions of no WPI perpendicular energy is converted to parallel energy due to the mirror

force and the distribution functions are elongated in the parallel direction and reduced in the perpendicular direction. Centrifugal acceleration reduces the distribution functions in the parallel direction.

Conclusion

In this thesis we studied the properties of outflowing O^+ and H^+ ions in the regions defined in Figure 3.1 above the polar cap using a semikinetic model. This model included the effects of ambipolar electric field , wave-particle interactions, and the mirror, gravitational, and centrifugal forces. The effect of centrifugal acceleration was simulated using three values of the ionospheric convection field: 0, 50, and 100 mV/m. Our conclusions are:

1. Centrifugal acceleration is significant for trajectories above the polar cap for altitudes above 4 R_E.

2. In regions where centrifugal acceleration is significant it has the effect of increasing the parallel bulk velocity of ions, and decreasing the parallel and perpendicular temperature. Its effect on the density of the ions depends on the saturation of outflowing ions at the exobase. If the species's outflow at the exobase reached an optimal value without the influence of centrifugal acceleration, then adding centrifugal acceleration lowers the density due to the conservation of flux. On the other hand, if there is a considerable amount of ions not able to overcome the potential barrier, then the effect of centrifugal acceleration would be to increase the number of outflowing ions and hence the density at higher altitudes.

3. The effect of centrifugal acceleration seems to be independent of the species in consideration except for the O^+ ions in the cusp and the H^+ ions at low altitudes in the NPC.

4. Bulk velocities and densities are highest in the cusp followed by the CPC followed by the NPC region.

5. The density of O^+ ions is much smaller than the density of H^+ ions at high altitudes.

   In an ongoing study our results are compared to the observations reported by *Nilsson et al.* (2012) and *Nilsson et al.* (2013). In another ongoing study we are varying the geophysical conditions, i.e. the diffusion coefficients and boundary conditions, and studying the effect of this variation on the outflow of the ions.

Bibliography

Andre, M. (1997), Waves and wave-particle interactions in the auroral region, *Journal of Atmospheric and Solar-Terrestrial Physics*, *59*(14), 1687–1712, doi:10.1016/S1364-6826(96)00173-3.

André, M., and A. Yau (1997), Theories and Observations of Ion Energization and Outflow in the High Latitude Magnetosphere, *Space Science Reviews*, *80*(1-2), 27–48, doi:10.1023/A:1004921619885.

Barakat, A., and J. Lemaire (1990), Monte Carlo study of the escape of a minor species, *Physical Review A*, *42*(6), 3291–3302, doi:10.1103/PhysRevA.42.3291.

Barakat, A. R., and I. A. Barghouthi (1994), The effect of wave-particle interactions on the polar wind O +, *Geophysical Research Letters*, *21*(21), 2279–2282, doi:10.1029/94GL01701.

Barakat, A. R., and R. W. Schunk (2006), A three-dimensional model of the generalized polar wind, *Journal of Geophysical Research*, *111*(A12), A12,314, doi:10.1029/2006JA011662.

Barakat, A. R., H. Thiemann, and R. W. Schunk (1998), Comparison of macroscopic particle-in-cell and semikinetic models of the polar wind, *Journal of Geophysical Research*, *103*(A12), 29,277, doi:10.1029/98JA02540.

Barghouthi, I., A. Barakat, and A. Persoon (1998), The Effects of Altitude-Dependent Wave Particle Interactions on the Polar Wind Plasma, *Astrophysics and Space Science*, *259*(2), 117–140, doi:10.1023/A:1001569207346.

Barghouthi, I. A. (1997), Effects of wave-particle interactions on H+ and O+ outflow at high latitude: A comparative study, *Journal of Geophysical Research*, *102*(A10), 22,065, doi:10.1029/96JA03293.

Barghouthi, I. A. (2008), A Monte Carlo study for ion outflows at high altitude and high latitude: Barghouthi model, *Journal of Geophysical Research*, *113*(A8), A08,209, doi: 10.1029/2008JA013274.

Barghouthi, I. A., and M. A. Atout (2006), Monte Carlo modeling of toroidal ion distributions and ion temperatures at high altitudes equatorward of the cusp: Effect of finite gyroradius, *Journal of Geophysical Research*, *111*(A3), A03,202, doi:10.1029/2005JA011437.

Barghouthi, I. A., A. R. Barakat, and R. W. Schunk (1993), Monte Carlo Study of the transition region in the polar wind: An improved collision model, *Journal of Geophysical Research*, *98*(A10), 17,583, doi:10.1029/93JA01190.

Barghouthi, I. A., A. R. Barakat, and R. W. Schunk (1994), A Monte Carlo simulation of the effect of ion self-collisions on the ion velocity distribution function in the high-latitude F-region, *Annales Geophysicae*, *12*(10/11), 1076–1084, doi:10.1007/s00585-994-1076-2.

Barghouthi, I. A., N. A. Qatanani, and F. M. Allan (2003), Monte Carlo Simulation of Boltzmann Equation in Space Plasma at High Latitudes, *Monte Carlo Methods and Applications*, *9*(3), doi:10.1515/156939603322728978.

Barghouthi, I. A., N. M. Doudin, A. A. Saleh, and V. Pierrard (2007), High-altitude and high-latitude O+ and H+ outflows: the effect of finite electromagnetic turbulence wavelength, *Annales Geophysicae*, *25*(10), 2195–2202, doi:10.5194/angeo-25-2195-2007.

Barghouthi, I. A., S. H. Ghithan, and H. Nilsson (2011), A comparison study between observations and simulation results of Barghouthi model for O+ and H+ outflows in the polar wind, *Annales Geophysicae*, *29*(11), 2061–2079, doi:10.5194/angeo-29-2061-2011.

Barghouthi, I. A., H. Nilsson, and S. Ghithan (2012), Comparison between the simulation results of Barghouthi model for ion outflows in the polar wind and auroral regions, *Journal*

of the Association of Arab Universities for Basic and Applied Sciences, *12*(1), 1–10, doi:10.1016/j.jaubas.2012.08.001.

Barghouthi, I. A., H. Nilsson, and S. H. Ghithan (2014), O+ and H+ ion heat fluxes at high altitudes and high latitudes, *Annales Geophysicae*, *32*(8), 1043–1057, doi:10.5194/angeo-32-1043-2014.

Baumjohann, W., and R. A. Treumann (1996), *Basic space plasma physics*, Imperial Coll.

Bouhram, M., B. Klecker, W. Miyake, H. Reme, J. Sauvaud, M. Malingre, L. Kistler, and A. Blagau (2004), On the altitude dependence of transversely heated O+ distributions in the cusp/cleft, *Annales Geophysicae*, pp. 1787–1798, doi:10.5194/angeo-22-1787-2004.

Chang, T., G. B. Crew, N. Hershkowitz, J. R. Jasperse, J. M. Retterer, and J. D. Winningham (1986), Transverse acceleration of oxygen ions by electromagnetic ion cyclotron resonance with broad band left-hand polarized waves, *Geophysical Research Letters*, *13*(7), 636–639, doi:10.1029/GL013i007p00636.

Chen, F. F., and A. W. Trivelpiece (1976), *Introduction to Plasma Physics*, vol. 29, 54 pp., doi:10.1063/1.3024417.

Chugunin, D. V. (2009), Characteristics of thermal ion outflows in the polar cap according to data of the Interball-2 satellite, *Cosmic Research*, *47*(6), 449–459, doi:10.1134/S001095250906001X.

Cladis, J. B. (1986), Parallel acceleration and transport of ions from polar ionosphere to plasma sheet, *Geophysical Research Letters*, *13*(9), 893–896, doi:10.1029/GL013i009p00893.

Demars, H. G., and R. W. Schunk (1992), Semikinetic and generalized transport models of the polar and solar winds, *Journal of Geophysical Research*, *97*(A2), 1581, doi:10.1029/91JA02378.

Demars, H. G., and R. W. Schunk (1994), A multi-ion generalized transport model of the polar wind, *Journal of Geophysical Research*, *99*(A2), 2215, doi:10.1029/93JA02356.

Demars, H. G., and R. W. Schunk (2002), Three-dimensional velocity structure of the polar wind, *Journal of Geophysical Research*, *107*(September), 1–21, doi:10.1029/2001JA000252.

Demars, H. G., A. R. Barakat, and R. W. Schunk (1996), Effect of centrifugal acceleration on the polar wind, *Journal of Geophysical Research*, *101*(A11), 24,565, doi:10.1029/96JA02234.

Demars, H. G., R. W. Schunk, and A. R. Barakat (1999), Comparing fluid and particle-in-cell solutions for the polar wind, *Journal of Geophysical Research*, *104*(A12), 28,535, doi:10.1029/1999JA900347.

Horwitz, J. L., and M. Lockwood (1985), The cleft ion fountain: A two-dimensional kinetic model, *Journal of Geophysical Research*, *90*(A10), 9749, doi:10.1029/JA090iA10p09749.

Horwitz, J. L., C. W. Ho, H. D. Scarbro, G. R. Wilson, and T. E. Moore (1994), Centrifugal acceleration of the polar wind, *Journal of Geophysical Research*, *99*(A8), 15,051, doi:10.1029/94JA00924.

Lemaire, J., W. Peterson, T. Chang, R. Schunk, A. Barakat, H. Demars, and G. Khazanov (2007), History of kinetic polar wind models and early observations, *Journal of Atmospheric and Solar-Terrestrial Physics*, *69*(16), 1901–1935, doi:10.1016/j.jastp.2007.08.011.

Liao, J., L. M. Kistler, C. G. Mouikis, B. Klecker, I. Dandouras, and J.-C. Zhang (2010), Statistical study of O + transport from the cusp to the lobes with Cluster CODIF data, *Journal of Geophysical Research*, *115*, A00J15, doi:10.1029/2010JA015613.

Lockwood, M., J. H. Waite, T. E. Moore, J. F. E. Johnson, and C. R. Chappell (1985), A new source of suprathermal O + ions near the dayside polar cap boundary, *Journal of Geophysical Research*, *90*(A5), 4099, doi:10.1029/JA090iA05p04099.

Moore, T. E., and J. L. Horwitz (2007), Stellar ablation of planetary atmospheres, *Reviews of Geophysics*, *45*(3), n/a–n/a, doi:10.1029/2005RG000194.

Nilsson, H. (2011), Heavy Ion Energization, Transport, and Loss in the Earth's Magnetosphere, in *The Dynamic Magnetosphere*, edited by W. Liu and M. Fujimoto, chap. 17, pp. 315–327, Springer, doi:10.1007/978-94-007-0501-2.

Nilsson, H., et al. (2004), The structure of high altitude O+ energization and outflow: a case study, *Annales Geophysicae*, *22*(7), 2497–2506, doi:10.5194/angeo-22-2497-2004.

Nilsson, H., et al. (2008), An assessment of the role of the centrifugal acceleration mechanism in high altitude polar cap oxygen ion outflow, *Annales Geophysicae*, *26*(1), 145–157, doi:10.5194/angeo-26-145-2008.

Nilsson, H., E. Engwall, A. Eriksson, P. A. Puhl-Quinn, and S. Arvelius (2010), Centrifugal acceleration in the magnetotail lobes, *Annales Geophysicae*, *28*(2), 569–576, doi:10.5194/angeo-28-569-2010.

Nilsson, H., I. A. Barghouthi, R. Slapak, A. I. Eriksson, and M. André (2012), Hot and cold ion outflow: Spatial distribution of ion heating, *Journal of Geophysical Research*, *117*(A11), A11,201, doi:10.1029/2012JA017974.

Nilsson, H., I. A. Barghouthi, R. Slapak, A. I. Eriksson, and M. André (2013), Hot and cold ion outflow: Observations and implications for numerical models, *Journal of Geophysical Research: Space Physics*, *118*(1), 105–117, doi:10.1029/2012JA017975.

Retterer, J., T. Chang, G. Crew, J. Jasperse, and J. Winningham (1987), Monte Carlo modeling of ionospheric oxygen acceleration by cyclotron resonance with broad-band electromagnetic turbulence, *Physical Review Letters*, *59*(1), 148–151, doi:10.1103/PhysRevLett.59.148.

Schunk, R. W. (1977), Mathematical structure of transport equations for multispecies flows, *Reviews of Geophysics*, *15*(4), 429, doi:10.1029/RG015i004p00429.

Seki, K., M. Hirahara, T. Terasawa, T. Mukai, Y. Saito, S. Machida, T. Yamamoto, and S. Kokubun (1998), Statistical properties and possible supply mechanisms of tailward cold O + beams in the lobe/mantle regions, *Journal of Geophysical Research*, *103*(A3), 4477, doi:10.1029/97JA02137.

Shelley, E. G., R. G. Johnson, and R. D. Sharp (1972), Satellite observations of energetic heavy ions during a geomagnetic storm, *Journal of Geophysical Research*, *77*(31), 6104–6110, doi:10.1029/JA077i031p06104.

Slapak, R., H. Nilsson, L. G. Westerberg, and A. Eriksson (2012), Observations of oxygen ions in the dayside magnetosheath associated with southward IMF, *Journal of Geophysical Research*, *117*(A7), A07,218, doi:10.1029/2012JA017754.

Slapak, R., H. Nilsson, and L. G. Westerberg (2013), A statistical study on O+ flux in the dayside magnetosheath, *Annales Geophysicae*, *31*(6), 1005–1010, doi:10.5194/angeo-31-1005-2013.

Tam, S., T. Chang, and V. Pierrard (2007), Kinetic modeling of the polar wind, *Journal of Atmospheric and Solar-Terrestrial Physics*, *69*(16), 1984–2027, doi:10.1016/j.jastp.2007.08.006.

Tsurutani, B. T., and G. S. Lakhina (1997), Some basic concepts of wave-particle interactions in collisionless plasmas, *Reviews of Geophysics*, *35*(4), 491, doi:10.1029/97RG02200.

Tsyganenko, N. (1989), A magnetospheric magnetic field model with a warped tail current sheet, *Planetary and Space Science*, *37*(1), 5–20, doi:10.1016/0032-0633(89)90066-4.

Tsyganenko, N. (1996), Effects of the solar wind conditions in the global magnetospheric configurations as deduced from data-based field models (Invited), *International Conference on Substorms*.

Tsyganenko, N. A. (1995), Modeling the Earth's magnetospheric magnetic field confined within a realistic magnetopause, *Journal of Geophysical Research*, *100*(A4), 5599, doi:10.1029/94JA03193.

Waara, M., R. Slapak, H. Nilsson, G. Stenberg, M. André, and I. A. Barghouthi (2011), Statistical evidence for O+ energization and outflow caused by wave-particle interaction in the high altitude cusp and mantle, *Annales Geophysicae*, *29*(5), 945–954, doi:10.5194/angeo-29-945-2011.

Walt, M. (2005), *Introduction to Geomagnetically Trapped Radiation*, Cambridge University Press.

Zhang, Q. H., R. Y. Liu, J. Y. Huang, M. W. Dunlop, Z. J. Hu, Y. V. Bogdanova, M. Lester, and H. Q. Hu (2008), Simultaneous Cluster and CUTLASS observations of FTEs on 11 February 2004, *Chinese Journal of Geophysics*, *51*(1), 1–11, doi:10.1002/cjg2.1188.

قوة الطرد المركزية على ارتفاعات عالية فوق الدائرة القطبية

اعداد: حمزة احمد محمد أبو ديه

اشراف: بروفيسور عماد برغوثي

ملخص:

في هذا البحث تم دراسة أثر قوة الطرد المركزية على حركة أيونات الاكسجين والهيدروجين على مسافات ما بين 1.7 و 15 من انصاف اقطار الأرض (متوسط نصف قطر الأرض 6371 كم) عن مركز الأرض داخل الدائرة القطبية. وذلك من خلال اجراء محاكاة باستخدام طريقة مونتي كارلو (Monte-Carlo simulation) . نموذج برغوثي كان يتضمن تأثير القوى الكهربائية الموازية للمجال المغناطيسي وقوة الجاذبية وتفاعل الأمواج مع الايونات بالاضافة الى قوة المرآة مع اعتبار المجال المغناطيسي قطري. تم تطوير هذا النموذج ليأخذ بعين الاعتبار قوة الطرد المركزية وتم استبدال المجال القطري بنموذج Tsyganenko T96 كما وتم تحديث الظروف الابتدائية للأيونات. ومن خلال هذا البحث وجدنا ان قوة الطرد المركزية على ارتفاع معين تزيد من السرعة الكلية للايونات وتقلل كل من درجة الحرارة الموازية والعمودية لكل من ايونات الهيدروجين والاكسجين. اما اثرها على الكثافة العددية للايونات فانها تتناقص بوجود قوة الطرد المركزية لايونات الهيدروجين بينما تزيد من الكثافة العددية لايونات الأكسجين.